4

Fourier Transform Infrared Spectroscopy for the Measurement of Spectral Line Profiles

Hassen Aroui[1], Johannes Orphal[2] and Fridolin Kwabia Tchana[3]
[1]*Laboratoire de Dynamique Moléculaire et Matériaux Photoniques, Université de Tunis, Ecole Supérieure des Sciences et Techniques de Tunis,*
[2]*Institute for Meteorology and Climate Research (IMK), Karlsruhe Institute of Technology (KIT),*
[3]*Laboratoire Interuniversitaire des Systèmes Atmosphériques (LISA), UMR CNRS 7583 Universités Paris Est Créteil et Paris- Diderot, Institut Pierre Simon Laplace,*
[1]*Tunisia*
[2]*Germany*
[3]*France*

1. Introduction

Our knowledge of the process of global change in Earth's atmosphere is primarily based on experimental observations made in situ or by remote-sensing. The data obtained reveal the state of the atmosphere and provide input data for validation of theoretical models of the atmosphere. In this context, high resolution molecular spectroscopy plays a key role as it is at the heart of optical remote sensing measurements. In fact, infrared spectroscopy is a powerful tool to identify and quantify atmospheric trace species, through the use of characteristic spectral signatures of the different molecular species and their associated vibration-rotation bands in the mid- or near-infrared. Different methods, based on quantitative spectroscopy, permit tropospheric or stratospheric measurements: in situ long path absorption, atmospheric absorption/emission by Fourier transform spectroscopy with high spectral resolution instruments on the ground, airborne, balloon-borne or satellite-borne measurements (Camy-Peyret et al., 2001). In all cases, the quality of the analysis and interpretation of atmospheric spectra requires reference spectroscopic information (positions, intensities, broadenings, profiles…) measured in the laboratory. Such information exists and is compiled in databases such as HITRAN, GEISA and ATMOS, available to the international scientific community.

Fourier Transform Infrared (FTIR) can be utilized to measure some components of an unknown mixture and is currently applied to the analysis of solids, liquids, and gases. The term FTIR refers to the manner in which the data is collected and converted from an interference pattern to a spectrum.

Fourier transform spectrometers have progressively replaced dispersive instruments for most applications due to their superior speed and sensitivity. They have greatly extended

the capabilities of infrared spectroscopy and have been applied to many fields that are very difficult or nearly impossible to study by dispersive instruments. Instead of analyzing each spectral component sequentially, as in a dispersive IR spectrometer, all frequencies are examined simultaneously in FTIR spectroscopy.

By interpreting the infrared absorption spectrum, information about the structure and the nature of the chemical bonds in a molecule can be determined. For most common materials, the spectrum of an unknown mixture can be identified by comparison to a library of known compounds.

The FTIR technique is a powerful tool for identification of chemical species and their structures, for interpretation of the atmospheric spectra by producing an infrared absorption spectrum that is like a molecular fingerprint. This technique can be used to identify chemicals from spills, paints, polymers, coatings, drugs, and contaminants. It can measure more than 120 gaseous pollutants in the ambient air (U.S. Environmental Protection Agency, 2011), such as carbon monoxide, sulfur dioxide, ozone, and many others. This technique can also quantify toxic organic pollutants, such as toluene, benzene, methanol etc. This quantification is based on the fact that every gas has its own specific spectrum. The FTIR sensor monitors the entire infrared spectrum and reads the different fingerprints of the gases present in the atmosphere.

FTIR spectroscopy is also extensively used in the study of absorption line profiles to determine spectroscopic parameters related to line broadening.

This chapter describes laboratory measurements of line parameters for atmospheric trace species, using Fourier transform spectroscopy in the infrared spectral range. An illustration is given with the example of atmospheric molecules such as NH3, OCS and CH3Br, for which we have determined line intensities, self- and foreign-gas broadening coefficients, pressure-induced line shifts, as well as line-mixing coefficients for these molecules for more than 300 rovibrational lines located in the spectral range 1000-3000 cm^{-1}, at room and low temperatures.

A non-linear least-squares multi-spectrum fitting procedure, including Doppler, and line-mixing effects, has been used to retrieve line parameters from more than twenty experimental spectra, recorded at different pressures of the molecules. The accuracies of the results are also estimated and discussed as a function of the measured parameter.

The results, obtained for several branches of the molecules considered here, will be presented and analyzed as a function of gas pressure, temperature, rotational quantum numbers and vibrational bands.

From the intensity measurements, we have determined effective transition dipole moments, vibrational band strengths as well as Herman–Wallis parameters for some bands taking into account Coriolis and *l*-type interactions.

For the NH_3 molecule, the results concerning line-mixing demonstrate a large amount of coupling between the symmetric and asymmetric components of inversion doublets. The pressure shift coefficients and line-mixing parameters are both positive and negative. Some groups of lines illustrate a correlation between line-mixing and line shift phenomena, demonstrated by a nonlinear pressure dependence of the line position.

Excluding the Introduction and the Conclusion, this chapter is divided into three sections. The FTIR spectroscopy technique is described in detail in section 2. In particular, the model used to describe the instrument line shape function of the Fourier transform spectrometer is presented. Measurement of line profiles using Fourier transform spectroscopy is presented in section 3. In this section, the measured broadening and shift coefficients, as well as line intensities and line-mixing parameters are presented and discussed. The rotational dependence of the pressure broadening coefficients is fitted using empirical polynomial equations to provide empirical interpolation and extrapolation models.

2. Fourier transform spectroscopy

2.1 Quantitative absorption spectroscopy

Infrared spectroscopy is the absorption measurement of different IR frequencies by a sample located in the path of an IR beam. Using various sampling accessories, the spectrometers can accept a wide range of sample types such as gases, liquids, and solids.

The basic principle for the evaluation in IR spectroscopy is the Beer-Lambert law which was defined in 1852. This law relates the absorption of light to the properties of the material through which the light is traveling. Absorption spectroscopy consists of the application of this law which illustrates that when traversing a measurement cell, the light intensity decreases exponentially:

$$I = I_0(\sigma)\exp\{-\alpha(\sigma)\ell\}, \tag{1}$$

where $\alpha(\sigma)$ (in cm^{-1}) is the absorption coefficient of the material, σ is the wavenumber (in cm^{-1}), ℓ is the absorption path length (in cm). $I_0(\sigma)$ and $I(\sigma)$ are the intensity of a collimated light beam (in Wm^{-2}) respectively before and after absorption by the sample.

The transmission spectrum $T(\sigma)$ is the ratio of $I(\sigma)$ by $I_0(\sigma)$:

$$T(\sigma) = \frac{I(\sigma)}{I_0(\sigma)}. \tag{2}$$

Eq. (1) can be expressed as a function of the absorption cross section $\sigma_e(\sigma)$ (in cm^{-2} $molecule^{-1}$).

$$I = I_0(v)\exp\{-\sigma_e(\sigma)N\ell\}. \tag{3}$$

N is the particle density (in molecule cm^{-3}). At standard conditions of pressure (P = 1 atm) and the temperature (T = 273.15 K), N is equal to the Loschmidt number[1] (Auwera, 2004):

$$n_L = 2.6867661\ (47) \times 10^{19}\ \text{molecule cm}^{-3}\ \text{atm}^{-1}.$$

[1] Computed from the value of the molar gas constant *R* available in February 2003 on the website of the Physics Laboratory of the National Institute of Science and Technology (http://physics.nist.gov/).

2.2 Fourier transform spectroscopy

2.2.1 Introduction

Since the invention of the first spectrophotometers in the beginning of 20th century, a rapid technological progress has occurred. The first-generation spectrometers were all dispersive with a prism or grating as dispersive elements. In the mid 1960s infrared spectroscopy has seen the advent of the Fourier transform spectrometer. These second-generation infrared spectrometers have significant advantages compared to dispersive spectrometers.

2.2.2 General description

The basic experimental set up of the Fourier transform spectrometer is constituted by the Michelson interferometer. As shown in Fig. 1, light from a source (S) is collimated and then divided at a beam splitter (L) into two beams of equal amplitude. These beams are reflected back on themselves by two separate mirrors, one fixed (M_2) and the other movable (M_1). Each single beam strikes the beam splitter again, where they are recombined and directed to the detector (D). The two components in the recombined beam interfere with each other and form a spot whose intensity depends upon the different paths traversed by the two beams before recombination. As one mirror moves, the path length of one beam changes and the spot on the detector becomes brighter and dimmer successively, in synchronization with the mirror position.

It should be noted that the same types of radiation sources can be used for both dispersive and Fourier transform spectrometers.

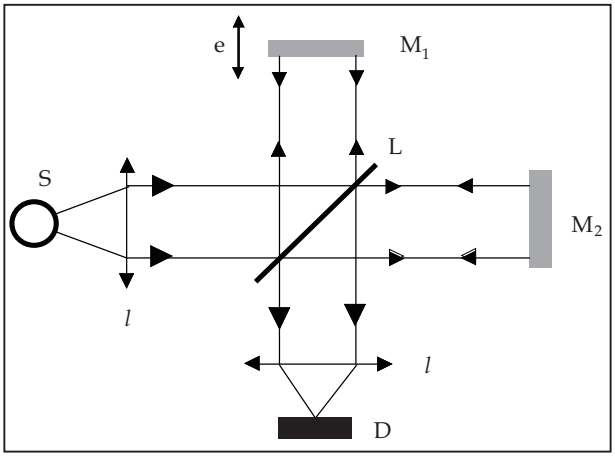

Fig. 1. Michelson interferometer showing three compartments: the radiation source (S), the detector (D), and the interferometer with its two mirrors M_1 and M_2 and its beam splitter L

2.3 Mathematic formulation

2.3.1 The interferogram expression

Fourier transform spectroscopy principles are extensively described in the literature (Bell, 1972; Davis et al., 2001; Griffiths & Haseth, 1986). Basically, a Fourier transform

spectrometer generates the quantity I′(δ) which is the cosine Fourier transform of the incident light beam of spectral irradiance B(σ) over a range of optical path differences δ defined by the positions of the moving mirror with respect to the fixed mirror (Bell, 1972):

$$I'(\delta) = \int_0^{\infty} B(\sigma)\left[1 + \cos(2\pi\sigma\delta)\right] d\sigma \,. \tag{4}$$

In FTIR spectroscopy, only the modulated part is retained:

$$I(\delta) = \int_0^{\infty} B(\sigma)\cos(2\pi\sigma\delta)\, d\sigma \,. \tag{5}$$

The real quantity I(δ) is called the interferogram. An example of such interferogram is shown in Fig. 2 for an infrared source, recorded from $-\delta_{max}$ to $+\delta_{max}$, where δ_{max} is the maximum optical path difference achieved.

The spectral distribution (spectrum) can be recorded by computation of the Fourier transform of I(δ):

$$\tilde{B}(\sigma) = \int_{-\infty}^{+\infty} I(\delta)\exp\{-i2\pi\sigma\delta\}\, d\delta \,. \tag{6}$$

This equation requires that the interferogram is known from $\delta_{max}=-\infty$ up to $\delta_{max}=\infty$. Since I(δ) can be split into the sum of even and odd functions (Brassewell, 1965):

$$I(\delta) = \frac{1}{2}\left[I(\delta) + I(-\delta)\right] + \frac{1}{2}\left[I(\delta) - I(-\delta)\right] = E(\delta) + O(\delta) \,. \tag{7}$$

Eq. (6) can be written as:

$$\tilde{B}(\sigma) = 2\int_0^{\infty} E(\delta)\cos(2\pi\sigma\delta)\, d\delta - 2i\int_0^{\infty} O(\delta)\sin(2\pi\sigma\delta)\, d\delta \,. \tag{8}$$

This equation shows that the observed spectrum B(σ) is real and even, if the interferogram is an even function. Only the side of the interferogram corresponding to $\delta \geq 0$ is recorded; the spectrum is then computed using the cosine Fourier transformation only.

2.3.2 Instrumental line shape function

When the spectral analysis takes into account experimental parameters such as the truncation of the interferogram, the finite size of the source, phase errors, optical misalignments, etc., an instrumental line shape function, $F_{App}(\sigma)$, is introduced, and the recorded spectrum can be written as:

$$\tilde{B}(\sigma) = B(\sigma) \otimes F_{App}(\sigma) \tag{9}$$

The symbol $\otimes$ means the convolution of B(σ) with $F_{App}(\sigma)$. In the following, we discuss the effect of $F_{App}(\sigma)$ on the recorded spectra.

2.3.3 Truncation of the interferogram

Mathematically, the truncation of the interferogram recorded up to a finite maximum optical path difference δ_{max} yields:

$$F_{App}(\sigma) = 2\delta_{max}\,\mathrm{sinc}(2\pi\sigma\delta_{max}), \tag{10}$$

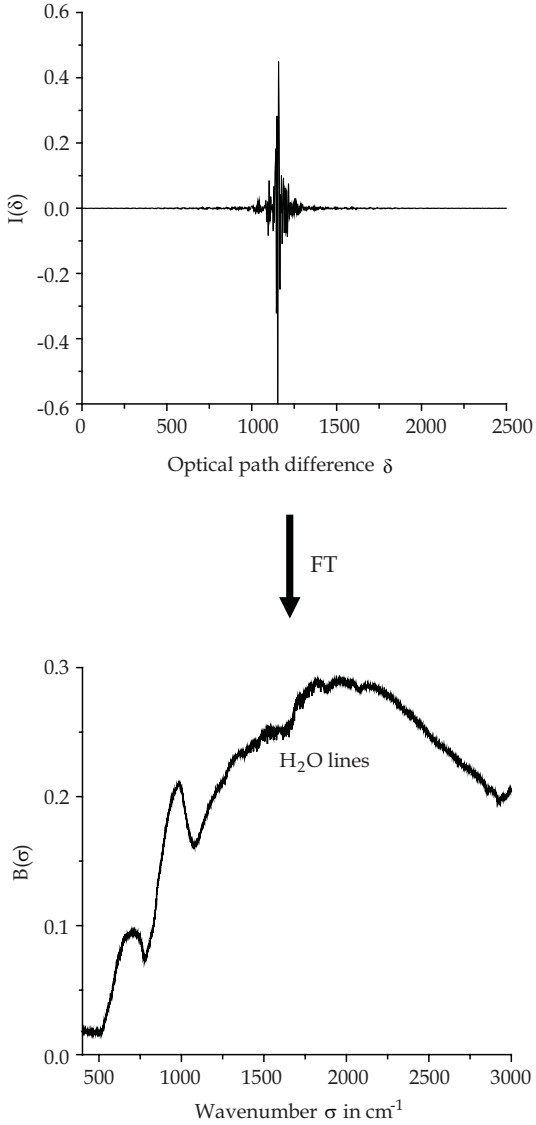

Fig. 2. Example of an interferogram and its spectrum calculated using a Fourier Transform algorithm

where sinc(x)=sin(x)/x. The full width at half maximum (FWHM) of this function defines the theoretical maximum spectral resolution R_{th} that can be achieved with a Fourier transform spectrometer (Bell, 1972):

$$R_{th} = \frac{1.2067}{2\delta_{max}}. \tag{11}$$

The sinc(x) function exhibits large oscillations: the amplitude of the first lobe is equal to 22% of the maximum amplitude of the function. These oscillations can be rather annoying for the spectral analysis since they lead to distortion of spectral lines. They can be reduced or eliminated through multiplication of the interferogram I(δ) with a so-called apodization function which decrease with increasing optical path difference, thus reducing the truncation effect of the interferogram at δ_{max}.

A typical apodization function is a triangle function whose Fourier transform is the $sinc^2(2\pi\delta_{max}\sigma)$ function. However, because R_{th} is inversely proportional to δ_{max}, apodization has the disadvantage of decreasing the spectral resolution. Then the apodized maximum spectral resolution achievable by a Fourier transform spectrometer is equal to the full width at half maximum of the $sinc^2(x)$ function.

$$R_{th} = \frac{1.79}{2\delta_{max}} \tag{12}$$

This definition of the resolution is used for Bruker FTIR spectrometers. For the Bomem instruments, $R = 0.5/\delta_{max}$ is used.

2.3.4 Detector non-linearity

For line intensity measurements, the major distortion of spectra may be due to the nonlinearities of the detector (MCT detectors are nonlinear). To remove these nonlinearities, some studies have been performed (Abrams et al., 1994; Auwera, 2004; Guelachvili, 1986). Abram et al. showed that the recorded interferogram can be described as power series of the true interferogram (Abrams et al., 1994). Later Auwera developed an algorithm based on Abram's work to avoid nonlinearities (Auwera, 2004).

This phenomenon is manifested when the detector is illuminated by a relatively intense source with large spectral coverage. This nonlinearity affects the interferograms near the zero optical path difference where the signal is the largest. Such behaviour affects consequently the entire spectrum.

Note that, using the sensitivity curve of the detector, one should be sure to remain permanently in the interval of linearity of detection by reducing the most possible the explored spectral region and by limiting the intensity of the source to avoid the effects of saturation of the detector. Since the true physical measured quantity is the interferogram, for broad band measurement in absorption spectroscopy, these effects will affect more strongly the center burst of the interferogramm, reducing artificially its amplitude where the signal is largest. Thus, one of the experimental signs signaling the presence of gross non-linearity effects is the appearance, after Fourier Transform, of an artefactual signal below the detector or beam-splitter cut-off (see for instance the curve below of Figure 2, where no signal should be present below 500 cm^{-1}).

2.3.5 Extended size of the source

The collimated beam inside the Michelson interferometer is produced using an extended source at the focus of a lens. This beam passes through an iris occulting part of the image of the source. Because of the finite size of this iris, the collimated beam is slightly divergent in the interferometer. When this effect is taken into account, the interferogram $I(\delta) = B\cos(2\pi\sigma_0\delta)$ of a monochromatic source at wavenumber σ_0 becomes

$$I(\delta) = B\frac{\pi d^2}{4F^2}\,\mathrm{sinc}\left(\frac{\pi d^2\sigma_0\delta}{8F^2}\right)\cos\left(2\pi\sigma_0\delta\left[1-\frac{d^2}{16F^2}\right]\right). \tag{13}$$

In this expression, d is the diameter of the iris and F the focal length of the collimating optic. This equation shows that the beam divergence has two effects:

- a change on the optical path difference $\delta' = \delta\left(1-\frac{d^2}{16F^2}\right)$. The first effect is easy to account for by using δ' in all calculations.
- a multiplication of the interferogram by a sinc(x) function at the wavenumber σ_0 of the source. This leads to a convolution of the spectrum with a box of width $\sigma_0 d^2/(8F^2)$.

2.3.6 Sampled interferogram and spectrum

First the interferogram is sampled at regular intervals as the moving mirror traverses the optical path difference δ. To avoid the loss of the signal information, for a spectrum with a $\Delta\sigma$ extend, the sampling step $\Delta\sigma$ must satisfy the Nyquist condition:

$$\Delta\delta < \frac{1}{2\Delta\sigma}. \tag{14}$$

Thus the continuous interferogram is multiplied by a sampling comb, modelled theoretically by a comb of delta functions. Sampling the interferogram has obvious effects such as replacing the integrals of Eqs. (6) and (8) by sums over the samples. The number of sample points in the spectrum is equal to $2\delta_{max}\Delta\sigma + 1$.

Practically in the spectrum the wavenumber interval between two points is equal to $\delta\sigma = \frac{1}{2\delta_{max}}$. Thus the spectral resolution is chosen such that there are at least two sample points per line width.

2.3.7 Zero filling

Zero filling is a data processing technique where zero points are added to the end of the interferogram before the digital Fourier transformation. It is the process of interpolating extra data points into a spectrum so that the spectral lines have a smoother shape with a better digital resolution, using the same Fourier coefficients. FTIR software automatically provides zero-filling by extending the length of an interferogram with a zero straight line. However there is no new information added to the spectrum.

Generally, the original interferogram size should always be at least doubled by zero filling, i.e. zero filling factor (ZFF) of two is chosen. Zero-filling is an interpolation that does not affect the instrument line-shape, and in most cases, is therefore superior to polynomial or spline interpolation methods that are applied in the spectral domain.

2.3.8 Phase errors

In Fourier transform spectroscopy interferograms are apodized prior to the transformation and the calculated spectrum is phase corrected. If the zero point for the Fourier transformation is displaced, a phase error occurs because the apodization remains fixed while the interferogram is shifted by the phase correction. To avoid distortions of the spectrum resulting from phase errors, double-sided interferograms are needed. In practice, single-sided interferograms are recorded double-sided on a small range of optical path difference, allowing determination of the phase error. In such a case, the phase error is determined at low resolution, typically about 1 cm^{-1} or less. This is not a problem because it varies only slowly with wavenumber.

2.4 FTIR advantages

Compared with the dispersive spectrometer, the FTIR instrument has several advantages:

- Better speed and sensitivity: A complete spectrum is obtained during a single scan of the moving mirror, while the detector observes all frequencies simultaneously. This is called the "Felgett advantage".
- The so-called "Jaquinot advantage" consists of an increase of the optical throughput. A circular optical aperture is used in FTIR systems. The beam area of a Fourier transform instrument is usually about 100 times larger than the small slit width of a dispersive spectrometer. Thus, more radiation energy is made available. This constitutes a major advantage for many samples that are energy-limited.
- The so-called "Connes advantage" consists of the use of a helium neon laser as the internal reference. This source radiation provides an automatic and stable calibration for all wavelengths. This eliminates, to some extent, the need for external calibration sources.
- FTIR spectrometers are usually equipped with a powerful, computerized data system. It can perform a wide variety of data processing tasks such as Fourier transformation, interactive spectral subtraction, baseline correction, smoothing, integration, spectral line fits and library searching. Development of the fast Fourier transform algorithm (Cooley and Tukey, 1965) has facilitated these tasks and reduced the computation time.

3. Measurement of line profiles using Fourier transform infrared spectroscopy

3.1 Introduction

Analysis of line profiles are useful for atmosphere monitoring and studying the evolution of its composition including chemical trace species related to the reduction in stratospheric ozone, starting from the analysis of observations obtained by infrared spectroscopy. The retrieved spectroscopic parameters are indispensable for the interpretation of high-resolution infrared spectra of gaseous species, and are of increasing importance for qualitative and

quantitative applications of spectroscopy. Also the pressure effects of gases on spectral lines are of significant interest in modeling and interpretation of radiative transfer calculations in climate models. In this context, inversion of atmospheric spectra to determine column densities of trace atmospheric species requires accurate knowledge of spectroscopic parameters. The needed parameters are, among others, line positions, line intensities, lower state transition energies and line widths as a function of temperature and quantum numbers.

However, spectroscopic information contained in the databases such as HITRAN09 (Rothman et al., 2009), GEISA (Jacquinet-Husson et al., 2005), JPL (Pickett et al., 1998) and the more specialized MASTER (Perrin et al., 2005), are often still partly incomplete, e.g. for some species or transitions, experimental or theoretical line pressure shift and line-mixing parameters are missing. For this reason, Fourier transform spectroscopy is extensively used to generate these parameters. Compared to diode laser spectrometers, FT spectrometers have the advantage of recording spectra over a large frequency range.

In this context, we present in the following Fourier transform measurements of NH_3, CH_3Br and OCS line profile parameters (line intensity, line width, line-mixing and line shift).

When the gas pressure increases, inelastic collisions transfer populations from one radiative state to another. At low pressure, the lines are isolated; this effect gives a line broadening and shift proportional to the pressure. At high pressure the lines are overlapped, interference effects occur between adjacent lines. The resulting profile can no longer be described by the superposition of Lorentzian profiles. In this case, in addition to the previous parameters, one must determine the line-mixing coefficients.

A large amount of laboratory data using various spectroscopic techniques of increasing precision has been assembled over the last two decades. Among the various molecular species, ammonia (NH_3) is probably one of the most investigated species. This molecule has always played an important spectroscopic role because of its inversion spectrum and its large molecular dipole, which are important properties for theoretical models. Moreover, ammonia is present in many planetary atmospheres (Ho & Townes, 1983; Kunde et al., 1982). It is also commonly used as an interstellar thermometer and is considered as an industrial and biological pollutant (Brassington, 1988).

The methyl halides (i.e. CH_3Cl, CH_3Br, and CH_3I) have been the subject of very detailed studies of the Earth's atmosphere. They are atmospheric components which take part in atmospheric photochemical reactions. Methyl bromide (CH_3Br) is a halogen chemical compound used in agriculture as a plant fungicide, and automobile using leaded petrol (Thomas et al., 1977).

This molecule significantly contributes to ozone depletion since CH_3Br is dissociated by UV radiation, producing Br radicals that catalyze the destruction of ozone (McElroy et al., 1986). These bromide atoms are far more destructive of ozone than the chlorine atoms coming from the chlorofluorocarbons compounds (CFC) (Kurylo & Rodriguez, 1998). For this reason, since 2005 the use of CH_3Br has been prevented under the Montreal protocol. Despite the important role of CH_3Br in the atmosphere, no spectroscopic data on CH_3Br is available in the main databases (Jacquinet-Husson et al., 2005; Perrin et al., 2005; Pickett et al., 1998; Rothman et al., 2009).

Carbonyl sulfide (OCS) is one of the principal and most long-lived reservoirs of sulfur in the Earth's troposphere (Watts, 2000) and has been detected in different astrophysical objects (the atmosphere of Venus (Bezard et al., 1990), the Orion molecular clouds (Evans et al., 1991), the comets Hyakutake and Hale-Bopp (Dello Russo et al., 1998; Woodney et al., 1997), and the starburst galaxies (Martin et al., 2005; Mauersberger et al., 1995)).

3.2 Experimental set-up

The results presented and discussed in the following are obtained using spectra recorded with the high resolution Bruker IFS125HR Fourier transform spectrometer (an upgraded version of the previous version, IFS120HR) located at the LISA facility, in Créteil. A general view of the laboratory is presented in Fig. 3. It shows the Fourier transform spectrometer Bruker IFS125HR, two multiple-reflections (white-type) Pyrex absorption cells and a gas handling system. The Fourier transform spectrometer is characterized by a maximum optical path difference (MOPD) of up to 473.68 cm (maximum resolution = 0.0019 cm^{-1}).

The instrument has all the equipment and accessories required to operate from the far infrared (20 cm^{-1}, 500 microns) to the ultraviolet region (45000 cm^{-1}).

Fig. 3. View of the laboratory showing the Fourier transform spectrometer Bruker IFS125HR, two multiple-reflections Pyrex absorption cells and a gas handling system including a turbomolecular pump. In the back is an optical table with a difference frequency generation (DFG) laser system developed at LPPM in Orsay and LISA in Creteil

The two multiple reflections cells are of the so-called White-type. They consist of a Pyrex tube containing the mirrors separated by 20 and 80 cm, respectively, thus providing base lengths of 0.849 and 3.249 m (this value takes into account the distance between the surface of the field mirror and the windows of the cell (2 × 2.45 cm)). The largest path length that one can achieve is 7.249 m with the short cell and 32.049 m with the long one. The temperature of the sample in these cells is well defined by an air-conditioning system regulating the temperature of the room, with an uncertainty of ± 1 K.

The gas handling system is made of stainless steel tubing and can be evacuated to less than 10^{-6} mbar by a Pfeiffer Turbomolecular Pumps. Commercial gas lecture bottles with pure samples or buffer gases like N_2, He, Ne, Ar etc. can be connected to the system to allow transfer of the gases to be studied into the absorption cells.

Fig. 4 presents the optical design of the Fourier transform spectrometer Bruker IFS 125HR. This instrument is a fast-scanning, asymmetrical Michelson interferometer, characterized by a resolving power better than one million. Four different parts can be distinguished: the source compartment (bottom right), the interferometer itself (above the sources), the sample position (where short path absorption cells are placed) and detector compartment. The whole optical path is maintained under vacuum (pressure below 0.06 mbar). This instrument provides three different sources, a high-pressure Hg lamp for the far-infrared, a globar (Silicon Carbide, SiC) heated to about 1100 K for the mid-infrared, and a tungsten lamp for the near-infrared and visible regions. An external light beam can also enter the instrument through the input port. The light is focused onto an iris, whose size ranges from 0.5 to 12 mm (aperture changer).

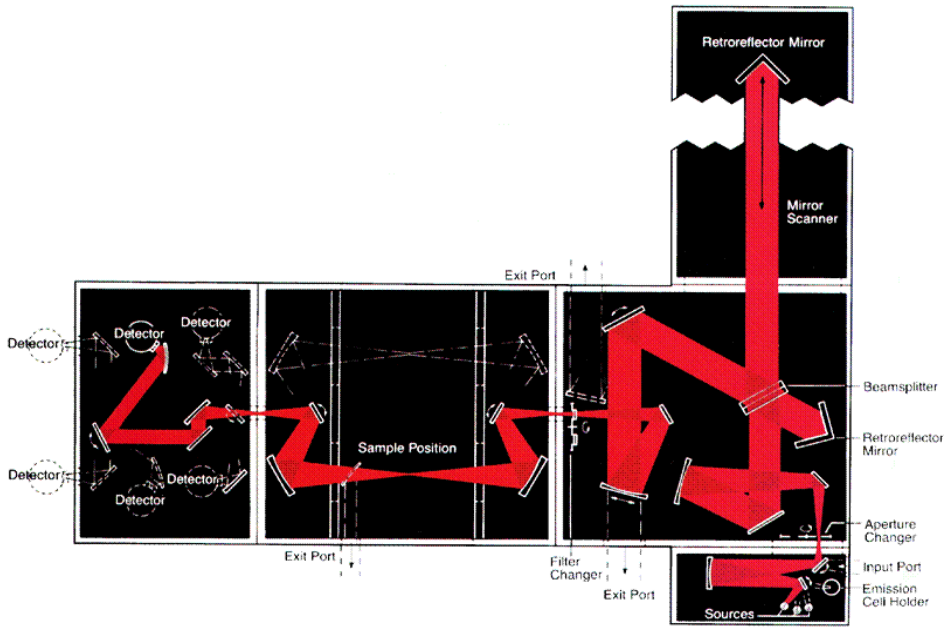

Fig. 4. Optical scheme of the Bruker IFS125HR Fourier transform spectrometer

The light is then collimated into a 7 cm diameter beam, sent into the Michelson interferometer. Various beam splitters, made of Mylar, KBr/Ge, CaF_2/Si and Quartz/TiO_2 are available, and used for different spectral regions. Exiting from the interferometer, the light is focused through an optical filter and then through the secondary iris. The beam then goes through the sample. Finally, the beam reaches the detectors compartment. We use four detectors, a Si bolometer operating at 4.2 K, a HgCdTe (MCT) detector, and an InSb detector, both cooled to 77 K, and a Si photodiode at room temperature.

For the studies of the OCS molecule, this spectrometer was equipped with a KBr/Ge beamsplitter, Globar source (Silicon Carbide, SiC), an InSb detector cooled at 77 K, and optical and electronic filters covering the spectral region 1850 - 2150 cm^{-1}.

For NH_3 and CH_3Br spectra in the region 1000-1800 cm^{-1}, we used also a liquid nitrogen-cooled HgCdTe detector. These spectra were recorded with an aperture diameter of 1.15 mm, 40 kHz scanner frequency, and a maximum optical path difference MOPD = 225 cm for OCS and NH_3, and 450 cm for CH_3Br. According to the Bruker definition this corresponds to a resolution of 0.004 cm^{-1} for OCS and NH_3 spectra and 0.002 cm^{-1} for CH_3Br.

A White-type multipass absorption cell, made of Pyrex glass and equipped with CsBr windows, was used to record OCS spectra broadened by O_2 and N_2. The cell is in thermic equilibrium with the air conditioned room with a temperature stabilized at 295 K. For NH_3 self-broadening experiments the gas was contained in a stainless steel gas cell equipped with CaF_2 windows with a path-length of 2.5 cm. For NH_3-H_2 collisions, the gas mixture was contained in a Pyrex cell, with a path length of 15 cm, equipped with ZnSe windows. For CH_3Br spectra, a multipass cell, of 1m base length equipped with KCl windows, was used for a total absorption path of 415 cm.

For self-broadening studies, the cell was filled with an increasing pressure of the active gas. For foreign gas broadenings, the cell was first filled with the active gas, then, after thermalization, the absorption cell was filled with an increasing pressure of perturber gas.

The following procedure was used for measurements: First a background spectrum was collected while the cell was being continuously evacuated. Next, the cell was filled with the considered gas at an increasing pressure. For OCS or NH_3 perturbed by N_2 or H_2, the pressure of these gases was added in stages leading to a series of at least 6 pressures. Table 1 summarizes the experimental conditions of the spectra recorded for OCS-N_2 and OCS-O_2 collisions. The number of spectra for each gas is chosen in order to have sufficient information on all line parameters when analyzing a transition using the multi-spectrum fitting procedure. The sample pressure in the cell was measured using a calibrated MKS Baratron capacitance manometers (2, 10, 100, 1000 Torr full scale) each of them characterized by its stated uncertainty according to the manufacturer. For all these manometers the uncertainty is less than 1 %. The spectra were recorded at a stabilized room temperature of 295 K with an uncertainty of ± 1 K. All spectra were ratioed against the empty cell, single-channel background spectrum which was taken in order to ensure the best possible signal-to-noise in the ratioed spectra. The spectra were the result of the co-addition of a large number of scans (interferograms). For CH_3Br spectra, the number of scans was 200. Every scan has been individually transformed to spectrum using the Fourier transform procedure included in the Bruker software OPUS package (Wartewig, 2003), selecting a Mertz phase error correction (Griffiths & Haseth, 1986; Mertz, 1965).

Optical path (m)			3.249	
Resolution (cm^{-1})			0.004	
Maximum optical path difference (cm)			225	
Collimator focal length (mm)			418	
Aperture diameter (mm)			1.15	
Useful spectral domain (cm^{-1})			1850-2150	
Spectrum number	**OCS-N_2**		**OCS-O_2**	
	OCS pressure (Torr)[a]	**N_2 pressure (Torr)[a]**	**OCS pressure (Torr)[a]**	**O_2 pressure (Torr)[a]**
1	0.0859 (1)	7.74 (2)	0.0754 (1)	5.80 (1)
2	0.0859 (1)	15.05 (4)	0.0754 (1)	13.98 (3)
3	0.0859 (1)	25.53 (6)	0.0754 (1)	22.09 (6)
4	0.0859 (1)	34.89 (9)	0.0754 (1)	32.41 (8)
5	0.0859 (1)	46.90 (1)	0.0754 (1)	51.80 (1)
6	0.0859 (1)	60.00 (2)	0.0754 (1)	83.20 (2)

[a] The values given in parentheses correspond to the estimated errors.

Table 1. Experimental data

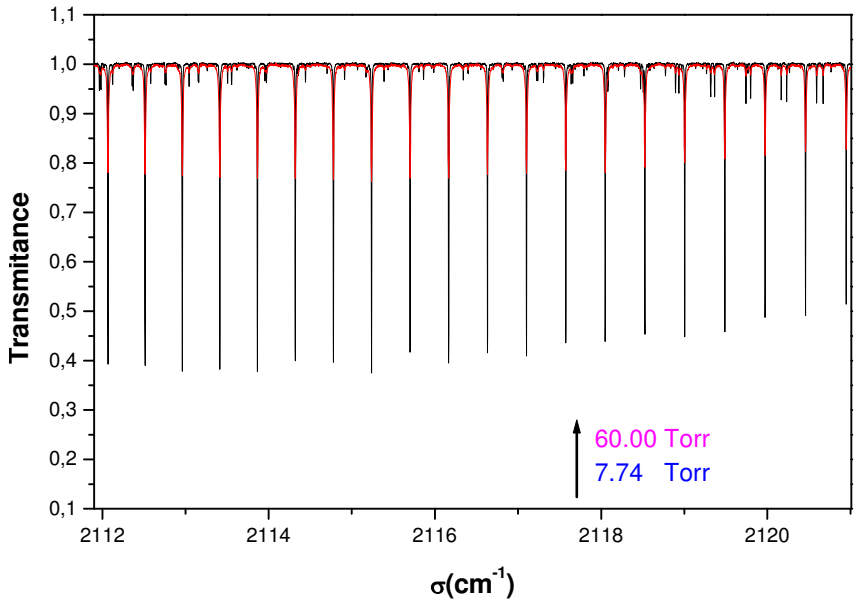

Fig. 5. Transmittance spectrum of OCS around 2116 cm^{-1} showing some lines of the R branch of $4\nu_2$ band broadened by N_2. The pressures are 0.086 Torr of OCS, and 7.74 and 60.00 Torr of N_2

The OCS spectra were calibrated with residual CO_2 and H_2O lines observed in the spectra. For CH_3Br the calibration was done using the low pressure ν_2 band spectrum of NH_3.

3.3 Fitting procedure

For OCS and NH_3 spectra, the analyses have been done taking into account interference effects. Thus within the impact theory of the spectral line shape and for moderately a overlapping line at low pressure considered for these molecules, the collisional absorption coefficient $\alpha(\sigma)$ could be written as (Gentry & Larrabee Strow, 1997; Lévy et al., 1992; Pine, 1997; Rosenkranz, 1975; Thibault et al., 1992):

$$\alpha(\sigma) = \frac{P_{NH_3}}{\pi} \sum_{\text{lines } k} S_k \frac{PY_k(\sigma - \sigma_k) + P\gamma_k}{(\sigma - \sigma_k)^2 + (P\gamma_k)^2}, \tag{15}$$

where k represents the line $v_i J_i K_i \rightarrow v_f J_f K_f$, S_k its intensity, σ_k its wavenumber, γ_k its halfwidth and Y_k its line mixing parameter related to the off diagonal element of the relaxation matrix.

Spectra were analyzed by means of nonlinear least squares fitting procedures, using the following theoretical expression $\tau^C(\sigma)$ for the transmission and the collisional absorption coefficient in Eq. (15):

$$\tau^C(\sigma) = \int_{-\infty}^{+\infty} F_{App}(\sigma - \sigma') \times \exp\left[-\ell \times \int_{-\infty}^{+\infty} \alpha_{Dop}(\sigma' - \sigma'') \times \alpha(\sigma'') \times d\sigma''\right] \times d\sigma', \tag{16}$$

where α_{Dop} is the Doppler profile, F_{App} is the Fourier transform instrument function with a gaussian shape and ℓ is the cell length. Eq. (16) is a convolution of the collisional absorption coefficient with the instrument function and the Doppler profile.

Otherwise the collisional parameters for a given temperature have been deduced by means of nonlinear least square multipressure fitting in which all spectra at various pressures are successively adjusted using Eq. (16). For a line k, the parameters deduced from the fits are $P\gamma_k$, σ_k, S_k and PY_k. These spectroscopic parameters have been iteratively varied by a fitting program to obtain the best agreement between the experimental and calculated absorption coefficients.

Because of the spectral density for the bands of the molecules considered here and the strong values of the self-broadening coefficient, a line by line study could not have been possible with the relatively high pressure, so the line parameters were derived using the multi-spectrum fitting method applied to the measured shapes of the lines, including the interference effects caused by the line overlaps.

An example of a multi-spectrum fit in the case of $^{P}_{a}P(8,7)$ and the two components of the $^{P}_{as}P(8,8)$ doublet all pertaining to the ^{P}P branch of the ν_4 band is given in Fig. 6 with the corresponding pressures. Plots (a) and (b) show that the overlapping increases with NH_3 pressure. They also demonstrate clearly the influence of line-mixing in the overlapped contours as illustrated by large discrepancies obtained when this process is disregarded in Fig. 6(a).

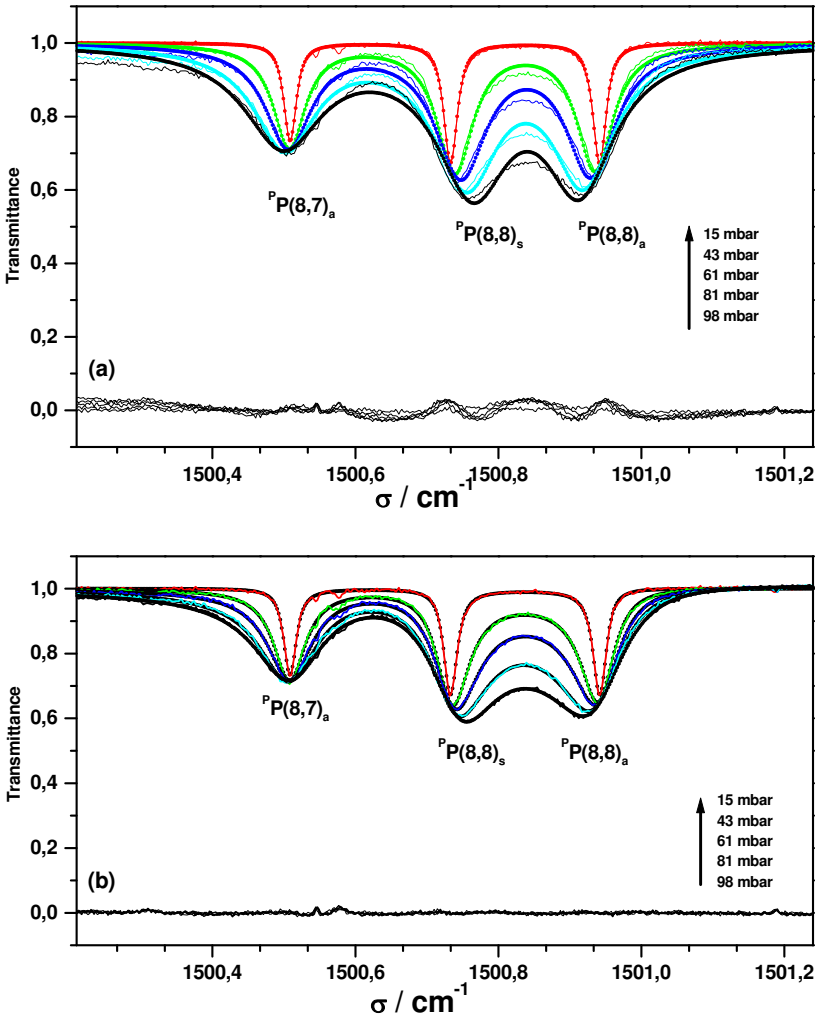

Fig. 6. Graphic demonstration of line-mixing obtained for pure NH_3 spectra for $^{P}_{a}P(8,7)$ line and $^{P}_{as}P(8,8)$ inversion doublet of the ν_4 band at various pressures. (—) and (•) are the measured and calculated values, respectively. Measured minus calculated deviations are shown in the lower part of graphs. Plots (a) and (b) have been obtained without (Y=0) and with (Y≠0) the line-mixing, respectively. These plots illustrate the shift of $^{P}_{as}P(8,8)$ components line center towards each other

Fig. 7 shows the results of multi-pressure spectrum fits for the $^{Q}P_{79}(26,E,5)$ line in the ν_2 band of CH_3Br, self-broadened at 296 K at different pressures. In this figure symbols and (—) are, respectively, the calculated and measured values. This line profile was calculated using a Voigt function. Indeed, no characteristic signature due to the presence of collisional narrowing or line-mixing has been observed in any residual.

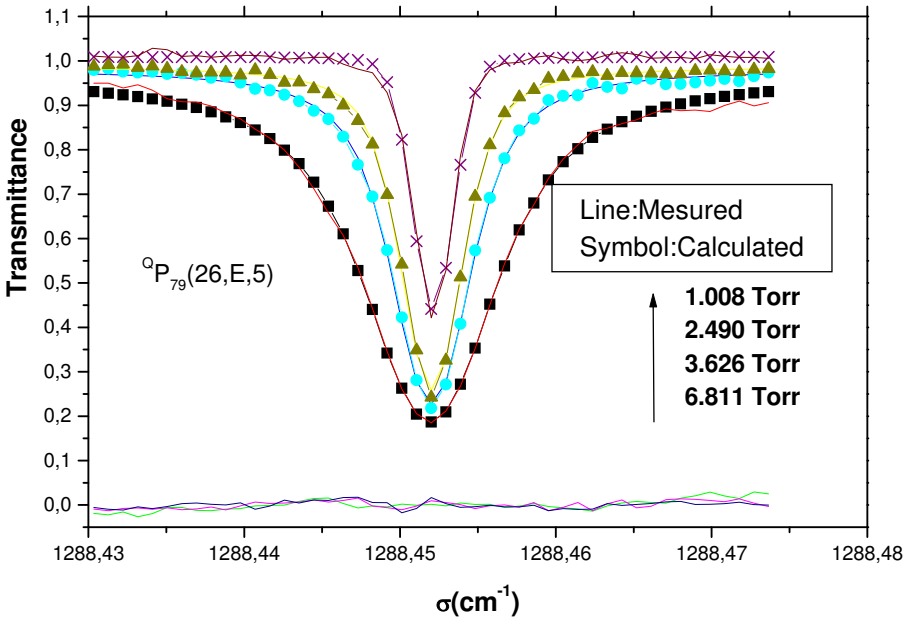

Fig. 7. Results of spectrum fits for the $^{Q}P_{79}(26,E,5)$ line in the ν_2 band of CH_3Br self-broadened at 296 K. (symbol) and (—) are, respectively, the calculated and measured values. Measured minus calculated deviations are shown in the lower part of the graph

3.4 Line intensities

3.4.1 Line intensity results

The line intensities presented here are for NH_3 in ν_2 and ν_4 band spectra. As shown in Fig. 8 for the $^{P_s}P(2,1)$, $^{P_s}P(3,1)$, $^{P_s}P(4,1)$, $^{P_s}P(6,1)$ and $^{P_s}P(7,1)$ lines of the ν_4 band, the intensity parameter S (cm^{-2}) derived from the fits is proportional to the real NH_3 pressure $P' = P \times 0.985$ (0.985 is the fractional abundance of NH_3 for the gas sample). The $^{P_s}P(5,1)$ line which has practically the same intensity value as the $^{P_s}P(3,1)$ line is not plotted. The line intensities S_0 (cm^{-2} atm^{-1}) are deduced from the slopes of the straight lines obtained from a linear least-squares procedure and the length ℓ = 2.5 cm of the absorption cell. The results are listed in Refs. (Aroui et al., 2003; Hadded et al., 2001) for symmetric and asymmetric transitions for the ν_2 and ν_4 bands of NH_3.

For the two bands, the intensities of transitions with a nuclear spin statistical weight of the lower level $g_s = 2$ for K = 3n (n = 1, 2,...) are larger than those with $g_s = 1$. S_0 increases with K for a given J when dividing by 2 the intensities of the lines with $g_s = 2$. However, for the ν_2 band when K is close or equal to J, line intensities exhibit a slight decrease. On the other hand, for a fixed value of K, S_0 decreases significantly as J increases. Otherwise the intensities of the asymmetric transitions are slightly larger than those of symmetric transitions. In the ^{P}P branch of the ν_4 band, line intensities also increase with K for a given J, but, as shown in Fig. 8, the evolution with J presents a maximum for J = 4 for the $^{P}P(J,K=1)$ lines and decrease monotonically for $K \geq 2$.

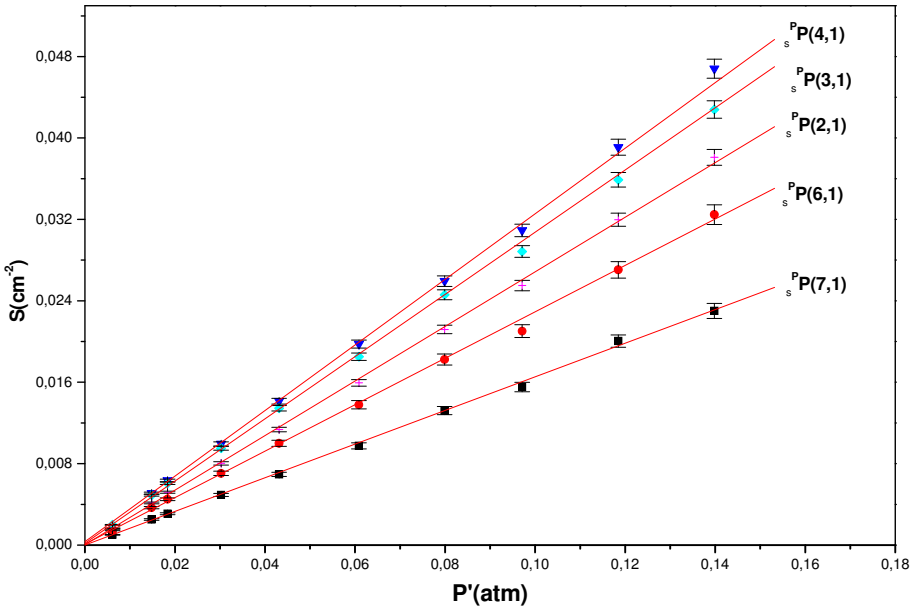

Fig. 8. Pressure dependence of the intensity parameter S for the $^{P}_{s}P(2,1)$, $^{P}_{s}P(3,1)$, $^{P}_{s}P(4,1)$, $^{P}_{s}P(6,1)$ and $^{P}_{s}P(7,1)$ lines in the ν_4 band of NH_3. The slopes of the best fit line represent the line intensity

As expected the line intensities in the ν_2 band (Aroui et al., 2003) are much larger than those reported previously (Aroui et al., 1998; Cottaz et al., 2001; Hadded et al., 2001) for the ν_4 band and also several times larger than the intensities in the ν_1 and ν_3 bands (Markov, 1993).

3.4.2 Vibrational transition moments and correction function

For NH_3 molecule, the effective transition dipole moments $R_{eff}(J,K)$ in the ν_2 band are derived from the line intensities S_0 such as (Aliev et al., 1987):

$$R^2_{eff}(J,K) = \frac{S_0 TQ \ \exp(E(J,K)/kT)}{3054.8 \ g_i \sigma \ \left[1-\exp(h\sigma/kT)\right] \ H_{JK}}, \quad (17)$$

where H_{JK} is the Höln-London factor (Aroui et al., 2003). σ is the wave number of the line under study. E(J,K) is the rotational energies of the lower level of the transitions. $Q = Q_r Q_v$ is the total partition function, with the rotational partition function $Q_r = 563.56$ at T = 295 K and the vibrational partition function $Q_v = 1.011$.

The effective transition dipole moments R_{eff}, determined from the observed line intensities using Eq. (17) show significant rotational dependencies (Aroui et al., 1998, 2003) which are mainly caused by vibration-rotation interactions (*l*-type interactions in the ν_4 band and Coriolis interaction between ν_4 and $2\nu_2$ bands): they decrease with J for a fixed value of K and increase with K for a given J.

For the interpretation of these dependencies, the zero-order theory, where the correction for vibration-rotation interactions is not included, cannot describe the transition dipole moment variations. By taking in to account the effects of these interactions, one can write

$$R_{eff}^2(J,K) = \left(R_0^v\right)^2 F_{HW}, \quad (18)$$

where R_0^v is the vibrational transition moment, and F_{HW} is the Herman-Wallis correction function describing the dependence of R_{eff} on J and K. For the ν_2 parallel band, for example, using the second-order development of Watson (Watson, 1992) we may write,

$$F_{HW} = \left\{1 + A^J m_J + A^K m_K + A^{JJ(Q)}\left[\overline{J(J+1)} - m_J^2\right] + A^{JJ(PR)} m_J^2 + A^{KK}\overline{K^2} + A^{JK} m_J m_K\right\}^2, \quad (19)$$

where the A's are correction parameters. For the R-transitions of this band, we have $m_J = J+1$, $m_K = 0$, $\overline{J(J+1)} = (J+1)^2$ and $\overline{K^2} = K^2$, thus we can write F_{HW} in the form:

$$F_{HW} = \left[1 + A^J(J+1) \;+\; A^{JJ(R)}(J+1)^2 \;+\; A^{KK}K^2\right]^2. \quad (20)$$

The correction parameters A^J, $A^{JJ(R)}$ and A^{KK} as well as the vibrational transition moment R_0^v, were determined, using linear least-squares fits, from the experimental values of effective transition moments. The resulting correction parameters and vibrational transition moments for the ν_2 band are listed in Table 2 along with the standard deviation of the fits (Aroui et al., 2003). In this table, the A^J and $A^{JJ(R)}$ parameters cannot be determined for ν_{2s}, since, for this partial band, the fits were performed only for 7 transitions pertaining to the $J = 10$ manifold, whereas for asymmetric ν_{2a} partial band the fits were performed for 62 transitions.

For the ν_4 band, the correction function, the vibrational transition moments and the correction parameters are reported previously (Aroui et al., 1998). For this band significant differences between the correction parameters obtained for the symmetric and asymmetric transitions, so one can determine the vibrational band strengths, S_{0S}^V and S_{0a}^V respectively, for the symmetric and asymmetric partial bands ν_{4s} and ν_{4a} of the ν_4 band. The values are reported in previous work (Aroui et al., 1998).

Parameter	s←a transitions	a←s transitions
R_0^v (D)	0.24604 ± 0.00209	0.23868 ± 0.00154
A^J	$(-3.88 \pm 1.47)\times10^{-3}$	—
$A^{JJ(R)}$	$(-1.57 \pm 0.72)\times10^{-4}$	—
A^{KK}	$(7.66 \pm 0.62)\times10^{-4}$	$(5.03 \pm 0.37)\times10^{-4}$

Table 2. Vibrational transition moments and Herman-Wallis correction parameters for the symmetric and asymmetric transitions of the ν_2 band of NH_3 (Aroui et al., 2003)

3.5 Pressure broadenings

3.5.1 Pressure broadening coefficients

For NH_3-H_2 collisions, a typical plot of $P\gamma$ versus the pressure P of hydrogen is shown in Fig. 9 for the $^{P_s}P(3,1)$ line of NH_3 in the ν_4 band at the temperatures 235 and 296 K. The gases

were contained in a 15 cm path-length Pyrex cell. One can observe that straight line fits go through the measured points very well. The pressure broadening coefficients γ for each temperature are determined as the slopes of the best-fit lines. This figure illustrates an increase of line width with H_2 pressure but a decrease of broadening coefficient as function of temperature (Nouri, 2004). This dependence is usually well represented by the simple power law

$$\gamma = \gamma(T_0)\left(\frac{T_0}{T}\right)^n, \tag{21}$$

where $\gamma(T_0)$ is the broadening coefficient at the reference temperature T_0 = 296 K. From the measured values of γ at the considered temperatures, one can determine the values of exponent n as the slope of the graphs of $ln\gamma(T)$ versus lnT. The straight lines obtained for all transitions validate Eq. (21) within the indicated range of T. The derived values of n are given in Ref. (Nouri, 2004) for the ${}^{P}P$, ${}^{R}P$, ${}^{P}R$, ${}^{R}Q$, ${}^{R}R$, and ${}^{P}Q$ branches in the ν_4 band and for R branch in the $2\nu_2$ band of NH_3.

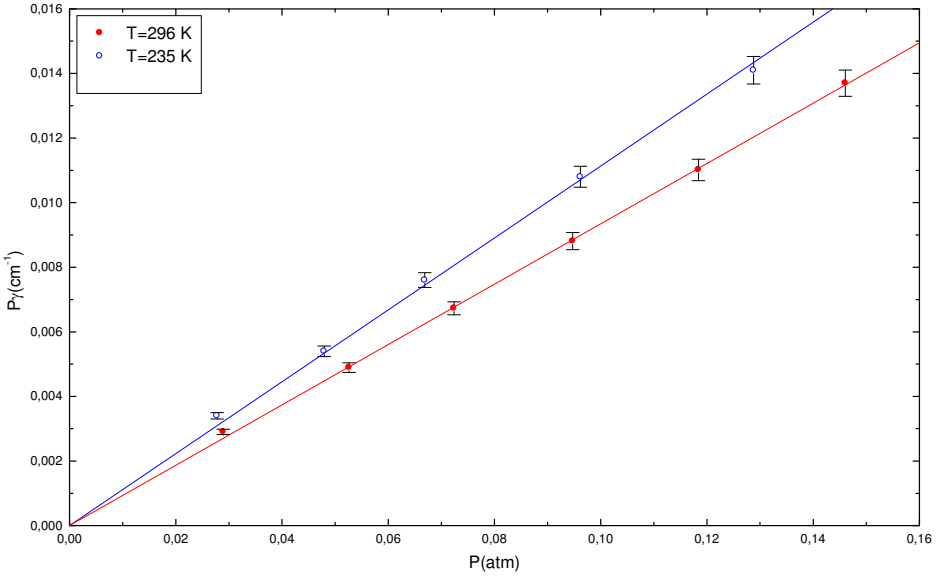

Fig. 9. Pressure dependence of the broadening line width $P\gamma$ for the ${}^{P_s}P(3,1)$ line of the ν_4 band perturbed by H_2; (o) T=235 K ; (•) T=296 K. The slope of the best fit line represents the broadening coefficient

As shown previously, distinctive dependence on the rotational quantum number m can be observed for the molecules considered here (Aroui et al., 2003, 2009; Bouanich et al., 1986; Cottaz et al., 2001; Domenech et al., 2000; Hadded et al., 2001; Koshelev et al., 2006, 2009; Markov et al., 1993; Mouchet et al., 1985). For OCS-N_2 and OCS-O_2 systems, Fig. 10 is a plot of the measured broadening coefficients versus |m| ($m = -J$ for $P(J)$ lines and $m = J + 1$ for $R(J)$ lines) for the P and R branches of the $4\nu_2$ band (Galalou et al., 2011). It shows the decrease of these coefficients with increasing |m|.

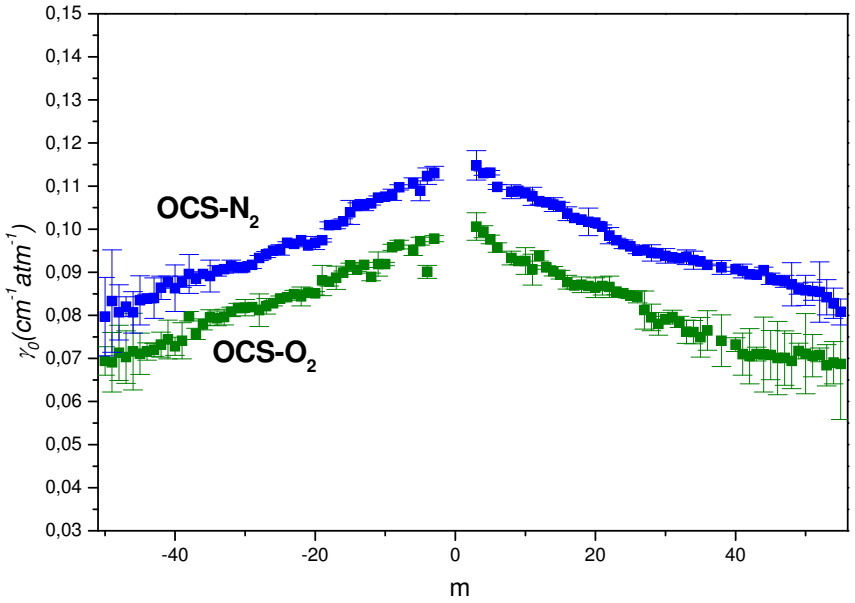

Fig. 10. Quantum number |m| dependence of the measured N_2, and O_2 broadening coefficients for P and R branches of the $4\nu_2$ band of OCS. Uncertainties become larger for high values of J (above 30) because of weaker line intensities

Contrary to the other symmetric top molecules, the broadening coefficients of NH_3 increase with K for a given J (Markov et al., 1993; Pine & Markov, 2004; Aroui et al., 2003, 2009). This behavior is more pronounced for the small J values. This increase could be related to the rotational energy separation between NH_3 levels which decrease with K. Note that the J = K lines have almost a constant value of broadening coefficient. These J and K dependencies have previously been observed in other bands (Hadded et al., 2001; Markov et al., 1993).

For CH_3Br molecule, previous works (Gomez et al., 2010, Jacquemart et al., 2007) report the observed and predicted self broadening coefficients of the ^PP, ^RQ and ^RR branches of the ν_6 band of CH_3Br. Fig. 11 shows that for a give K, the broadening coefficients of the ν_2 band increase with J in the interval $J \leq J_{max} = 20$ to nearly $\gamma = 0.45$ cm^{-1} atm^{-1} at $J = J_{max}$. Then these coefficients decrease at higher J values. The same trend is observed for the ν_6 band for K = 6 (Jacquemart et al., 2007). This pattern may be easily understood by considering the resonance condition that exists between the energy gaps of the two partners during collision. For the self broadening corresponding to the maximum contribution of the electrostatic interactions, J_{max} is given by the resonance condition (Giraud et al., 1971; Pourcin et al., 1981):

$$J_{max} \approx \frac{B_1}{B_2}\frac{\ell_1}{\ell_2} J_{2p} \tag{22}$$

J_{2P} is the most populated level of the perturbing molecule at the temperature considered (for CH_3Br at room temperature $J_{2p} = 18$). B_1 and B_2 are the rotational constants of the two

partners ($B_1 = B_2$ for CH_3Br auto-perturbed). The spherical harmonic orders ℓ_i depend on the nature of the interaction. Therefore for the self- broadening dominated by the dipole-dipole interaction ($\ell_1 = \ell_2 = 1$), the maximum of collision effectiveness is around $J_{max} = 18$ in reasonable agreement with the experimental observation in Fig. 11.

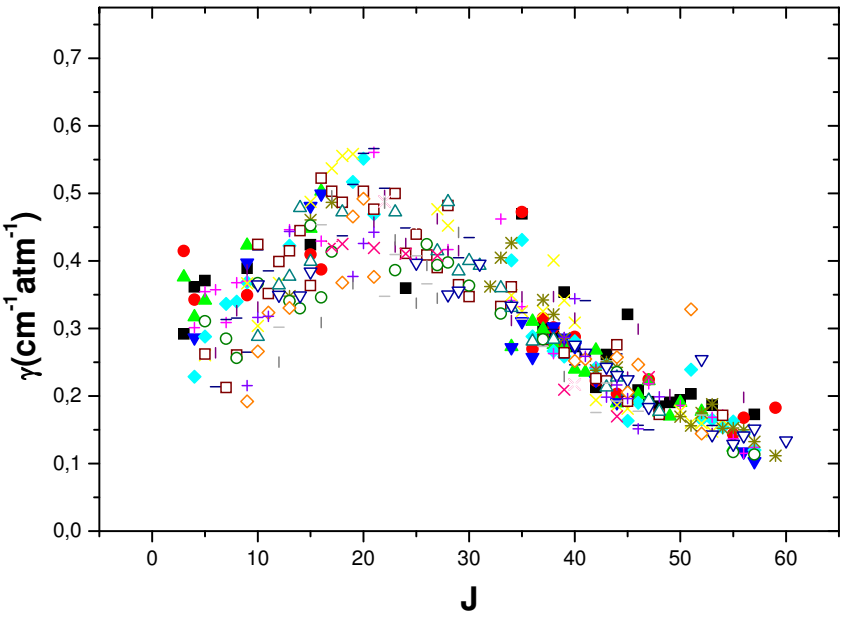

Fig. 11. Experimental self-broadening coefficients γ as function of the rotational quantum number J for the ν_2 band ^pQ branch of $^{12}CH_3{}^{79}Br$ and $^{12}CH_3{}^{81}Br$ for K=0 to 9. For a given J value, the symbols indicate the different K-lines for which measurements are performed

3.5.2 Polynomial fit of broadening coefficients

A constant need exists to examine the accuracy of the spectral line parameters listed in databases (Jacquinet-Husson et al., 2005; Perrin et al., 2005; Pickett et al., 1998; Rothman et al., 2009). For example, the NH_3 dataset in these databases has been revised by the inclusion of recent results (Brown & Peterson, 1994; Kleiner et al., 1999, 2003; Nemtchinov et al., 2004) but still needs to be improved and purged from possible errors in line parameters. However, generating the spectroscopic parameters represents a lot of work. This is why sometimes, due to the absence of the necessary information, the spectroscopic parameters obtained for lines of a given vibrational band are attributed to the corresponding lines of another band. For example, in the Hitran database, the air-broadening coefficients of OCS lines of the excited vibrational states are based on the ν_1 band measurement.

In this context, in order to provide empirical interpolation and extrapolation models for all spectral lines, some authors used empirical polynomial equations (Brown & Peterson, 1994; Aroui et al., 2009; Devis et al., 2002; Fabian & Yamada, 1999; Jacquemart et al., 2007) to fit the J and K dependencies of their pressure broadening coefficients.

Some least squares regressions fail to fit the observed values for particular quantum numbers. Other fits were satisfactory for nonpolar buffers, but fit poorly for self-broadening at low J quantum number.

In a recent paper (Aroui et al., 2009), the measured broadening coefficients of nine branches in the ν_2, $2\nu_2$ and ν_4 bands of NH_3 are fitted using the following equation.

$$\gamma(m,K) = \beta_0 + \beta_1 m + \beta_2 K + \beta_3 m^2 + \beta_4 K^2 + \beta_5 mK \quad (23)$$

The fitted parameters β_0, β_1, β_2, β_3, β_4 and β_5 are in unit of cm^{-1} atm^{-1}. They are given in Ref. (Aroui et al., 2009), along with the data points included in the fits. Most of the parameters are statistically well-determined and have remarkable regularities.

3.5.3 Vibrational dependence of pressure broadening

Some authors have discussed (Markov et al., 1993; Pine & Markov, 2004; Nemtchinov et al., 2004, Brown & Peterson, 1994; Cottaz et al., 2001; Aroui et al., 2009) the vibrational dependence of broadening coefficients. In most cases the comparison of the measured results for different bands exhibits little vibrational dependence. Within experimental error, the broadening coefficients of ammonia, for example, are only slightly greater in the ν_4 band than in the ν_2 and $2\nu_2$ bands. This is explained partially by the smaller splitting of the inversion doublets in the ν_4 band than in the ν_2 and $2\nu_2$ ones. For example, when the ν_2 and $2\nu_2$ bands are compared, the differences between line broadening coefficients with similar quantum numbers do not exceed 4% with a weighted average ratio $\langle \gamma(\nu_2)/\gamma(2\nu_2) \rangle = 1.031$.

However, for this molecule, Cottaz et al. (Cottaz et al., 2001) have highlighted a vibrational broadening effect when they compared their results for the R(3,1) line measured in six different vibrational bands. The present result for this line is slightly greater (3%) than that obtained by these authors.

For OCS-N_2 and OCS-O_2, pressure broadening coefficients in previous works for different bands (Bouanich et al., 1986; Domenech et al., 2000; Koshelev et al., 2006, 2009; Mouchet et al., 1985; Galalou et al., 2011), illustrate that no vibrational effect can be clearly identified. To clarify this effect, Ref. (Galalou et al., 2011) presents data of pressure broadening coefficients reported in earlier works. The observation of these results does not illustrate any clear differences between the bands.

3.6 Line-mixing effect

Line-mixing effects have received much less interest than line intensities and line broadening. This is mainly because they are rather small and their measurements are therefore difficult. However these spectroscopic parameters are necessary to detect molecules in tropospheric and planetary spectra, and to determine vertical concentration profiles. Moreover, even when laboratory measurements of these parameters are available, effects such as line-mixing may still require a sophisticated theoretical model in order to unravel observed spectra. When these effects are not negligible, the observed lineshapes exhibit significant deviations from the conventional Voigt profile, which may be attributed to line-mixing.

In the past decade, line-mixing effects have been examined for diverse molecules such as CO_2 (Ozanne et al., 1999), CH_4 (Pieroni et al., 1999), and OCS (Broquier & Picard-Bersellini, 1984). However for C_{3v} molecules the number of works is less. Measurements of these effects have been reported for CH_3F (Thibault et al., 1999), CH_3Cl (Hartmann et al., 1995) and CH_3Br (Tran et al., 2008). Otherwise, for NH_3, which presents line doubling due to its inversion motion, line-mixing effects were the subject of numerous works (Aroui et al., 1998, 2009; Dhib et al., 2007; Hadded et al., 2001). These works have clearly demonstrated the necessity of taking into account line-mixing in the molecular spectra.

We present below some line-mixing results for the NH_3 molecule. Plots of PY deduced from least squares fits (Eq. (16)) as a function of the NH_3 pressure P are shown in Fig. 12 for the components of the doublet, pertaining to the ν_4 band. The line-mixing parameter Y (in atm^{-1}) are determined as the slopes of the best-fit lines and are presented in Table 3 for the $^{P}P(5,K)$ and $^{P}P(6,K)$ manifolds of the ^{P}P branch of the ν_4 band of NH_3 at 295 K. The values given in parentheses correspond to the estimated errors corresponding to one standard deviation value.

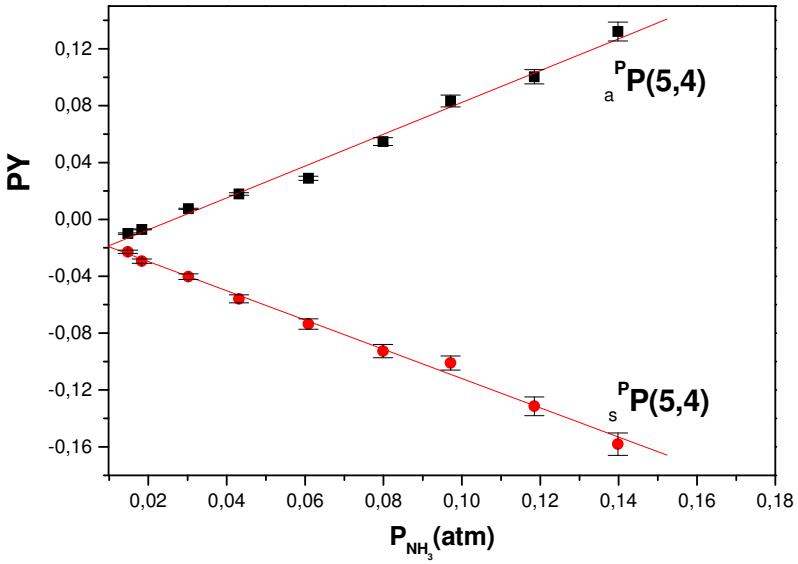

Fig. 12. Variation of PY as function of pressure P of NH_3 for the components of $^{P}_{as}P(5,4)$ doublet of the ν_4 band of NH_3 self-perturbed

This table shows that symmetric (s) and asymmetric (a) components of inversion doublets have opposite sign of Y. For numerous lines, Y appears to increase with K quantum number for a given value of J. This behavior could be explained in part by the decrease of the frequency difference between the manifold transitions with K, and particularly by the decrease of the $\Delta\sigma_0$ splitting inversion doublets components. This may be easily understood, since line-mixing parameter Y is inversely proportional to $\Delta\sigma_0$. Indeed, for a line k, Y_k is related to $\Delta\sigma_0$ and the off-diagonal element W_{lk} (line-coupling coefficient) of the relaxation matrix by (Gentry & Larrabee Strow, 1997; Pine, 1997; Pieroni et al., 1999):

$$Y_k = 2\sum_{l\neq k}\frac{d_l}{d_k}\frac{W_{lk}}{\Delta\sigma_0}\,. \tag{24}$$

$\Delta\sigma_0=\sigma_{0l}-\sigma_{0k}$ where σ_{0k} and σ_{0l} are the unperturbed positions of the k and l lines respectively; d_k and d_l are their reduced matrix elements of the dipole moment.

However, Table 1 of Ref. (Aroui et al., 2009) presents exceptions to this behavior: the parameter Y of ^{P}Q branch lines decreases with quantum number K. The situation is different for ^{R}Q and ^{R}R branches where no systematic dependence of interference parameter with J and K is observed.

Otherwise the $\Delta\sigma_0$ splitting could be large enough to contain lines other than those pertaining to the doublet of interest. So the line-mixing effects can occur not only between the two components of the doublets but also between more than two transitions, provided that the selection rules are valid.

On the other hand, the ν_2 band has a large inversion splitting, 35.7 cm^{-1} for the vibrational quantum number $v_2 = 1$. Thus the line-mixing is negligible and the inversion contribution to this effect should be smaller than for the ν_3 and ν_4 bands. In these bands (with very small inversion splitting, about 0.5 cm^{-1}) the line-mixing is essentially dominated by collisional transitions across the inversion doublets with the selection rules $\Delta J = 0$, $\Delta K = 0$ and $a\rightarrow s$. These two bands are thus the more appropriate to study line-mixing effects in the infrared bands of NH_3.

3.7 Pressure induced shift

Measurements of line-shifts have been investigated by numerous authors for various molecules. For NH_3, line shifts were measured by Dhib et al. in the ν_4 and $2\nu_2$ bands (Dhib et al., 2007), by Raynaud et al. in the ν_2 and $(2\nu_2-\nu_2)$ bands (Raynaud et al., 1994), by Baldacchini et al. in the ν_2 band, (Baldacchini et al., 1982), and by Aroui et al. in ν_2, $2\nu_2$ and ν_4 bands (Aroui et al., 2009).

For OCS, line shifts were measured by Domenech et al. (Domenech et al., 2000) for the $2\nu_3$ band, by Koshelev et al. in the ν_3 band (Koshelev et al., 2006) and in the ground vibrational state (Koshelev & Tretyakov, 2009), and by Babay (Babay, 1997) in the ν_2 band.

Fig. 13 shows typical plots of line shift $\sigma_k-\sigma_{0k}$ as function of NH_3 pressure for the $^{R}_{as}R(2,1)$ and $^{P}_{as}P(4,4)$ lines of the ν_4 band of NH_3. The self-shift coefficients δ_0 are determined as the slopes of the best-fit lines.

As may be seen by Fig. 13 and as illustrated by the results listed in Ref. (Aroui et al., 2009), shift coefficients are both positive and negative. A sample of these results is given by Table 3 for the ^{P}P branch of the ν_4 band. About two thirds of the lines have positive shifts, and the more bipolar shifts are obtained for the ν_4 band. Several symmetric and asymmetric components of the isolated inversion doublets in this band have opposite sign for the shift coefficients, so they appear to be shifting towards each other. As expected this mutual line-attraction is negligible in the ν_2 band, for which the splitting is very large compared to that of the ν_3 and ν_4 bands.

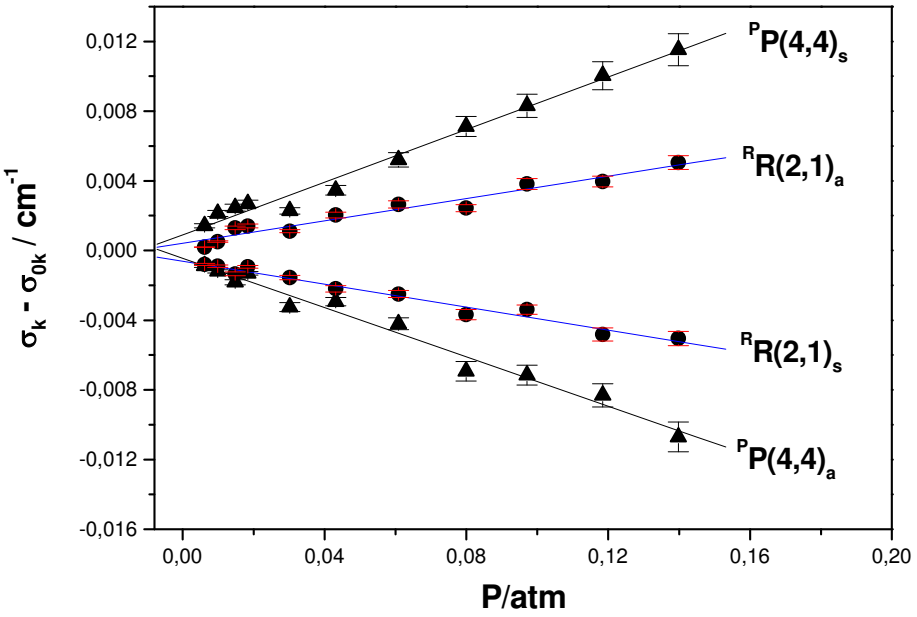

Fig. 13. Plots of the pressure-induced variation of σ-σ_0 versus NH_3 pressure P for the components of the doublets $^{R}_{as}R(2,1)$ and $^{P}_{as}P(4,4)$ of the ν_4 band of NH_3 self-perturbed

The self-shift coefficients of ammonia are larger than those obtained for other perturbers like He, H_2 and CO_2 (Hadded et al., 2001, Dhib et al., 2006) since the collisions in NH_3 are long range dipole-dipole collisions while the foreign gases collisions are shorter range collisions.

For all rotational lines of the molecules considered in this work, the shift coefficients do not reveal any systematic dependencies on the J and K quantum numbers with the exception seen in Table 3 for the NH_3 lines with K approaching J, for which the shift seems to increase with increasing K. For most of the lines of this molecule, the shifts are large, ranging from about -0.140 to +150 cm^{-1} atm^{-1}. The smallest one is $\delta_0 = 0.003 \pm 0.002$ cm^{-1} atm^{-1}. These shifts are in excellent agreement with the submillimeter measurement (Belov et al., 1982) of the ground state of NH_3 where $\delta_0 = 0.153 \pm 0.002$ cm^{-1} atm^{-1}, and somewhat larger than the ν_2 band diode laser measurement (Baldacchini et al., 1982) with $\delta_0 = 0.113 \pm 0.025$ cm^{-1} atm^{-1}. Similar large values of shifts are reported for other molecules such as CH_3CN studied by Rinsland et al. (Rinsland et al., 2008) using a multi-spectrum fitting technique.

For the R and P branches of the $4\nu_2$ band of OCS molecule perturbed by O_2 and N_2, the shift coefficients are mostly positive. The largest one is $\delta_0 = (17.91 \pm 3.02)\times10^{-3}$ $cm^{-1}atm^{-1}$, obtained for the R(51) line. These shifts are small compared with those of NH_3 and CH_3CN; this makes them difficult to measure as evidenced from their relatively large errors (Galalou et al., 2011).

In the $2\nu_3$ (Domenech et al., 2000), ν_3 (Koshelev et al., 2006) and ν_2 (Babay, 1997) bands of OCS molecule the shift coefficients were found negative for all studied lines. In the ground vibrational state (Koshelev & Tretyakov, 2009), the upper limits of the pressure shift

coefficient is $\delta_0 = \pm 0.38\ 10^{-3} cm^{-1} atm^{-1}$. This value is about 10 times smaller than those of the $4\nu_2$ band. These reasons, and the fact that the line shift coefficients do not illustrate any systematic variation with m, leads one to conclude that they depend on the vibrational band but are rotationally independent.

Lines	$\sigma_0(cm^{-1})$	$\delta_0(10^{-3}\ cm^{-1}\ atm^{-1})$	$Y(atm^{-1})$
$^{P}_{s}P(5,1)$	1536.2088	8.9 (5.3)	0.18 (0.02)
$^{P}_{a}P(5,1)$	1538.0102	-10.7 (5.7)	0.44 (0.10)
$^{P}_{s}P(5,2)$	1539.7596	10.7 (5.8)	0.43 (0.07)
$^{P}_{a}P(5,2)$	1541.0041	9.0 (5.0)	-0.25 (0.04)
$^{P}_{s}P(5,3)$	1542.9798	12.3 (4.1)	0.45 (0.02)
$^{P}_{a}P(5,3)$	1543.8550	-16.8 (6.6)	-0.42 (0.04)
$^{P}_{s}P(5,4)$	1545.8043	43.6 (5.6)	1.22 (0.06)
$^{P}_{a}P(5,4)$	1546.3315	-35.6 (6.6)	-1.10 (0.06)
$^{P}_{s}P(5,5)$	1548.1839	55.0 (10.0)	4.00 (0.09)
$^{P}_{a}P(5,5)$	1548.4290	-53.8 (10.9)	-4.16 (0.16)
$^{P}_{s}P(6,1)$	1519.6627	38.0 (6.3)	-0.62 (0.03)
$^{P}_{a}P(6,1)$	1522.3847	-13.5 (6.3)	0.74 (0.07)
$^{P}_{s}P(6,2)$	1522.7763	40.8 (6.0)	-0.81 (0.19)
$^{P}_{a}P(6,2)$	1524.7088	21.9 (4.7)	0.32 (0.05)
$^{P}_{s}P(6,3)$	1525.7625	47.3 (6.4)	-0.33 (0.03)
$^{P}_{a}P(6,3)$	1527.0615	18.4 (6.0)	-0.41 (0.03)
$^{P}_{s}P(6,4)$	1528.3774	18.6 (6.2)	0.74 (0.05)
$^{P}_{a}P(6,4)$	1529.2897	8.6 (4.7)	-0.67 (0.01)
$^{P}_{s}P(6,5)$	1530.6141	53.4 (5.5)	1.11 (0.04)
$^{P}_{a}P(6,5)$	1531.1591	-26.4 (7.3)	-1.28 (0.02)
$^{P}_{s}P(6,6)$	1532.4503	111.0 (9.4)	3.83 (0.11)
$^{P}_{a}P(6,6)$	1532.6830	-100.8 (13.4)	-4.03 (0.09)

Table 3. Self shift coefficients δ_0 (in $10^{-3}\ cm^{-1}\ atm^{-1}$) and self mixing parameters Y (in atm^{-1}) for the ^{P}P branch of ν_4 band of NH_3 at 295 K. The values given in parentheses correspond to the estimated errors expressed as one time standard deviation

It should be noted that one can determine the air-induced line shape parameters G (broadening coefficients, shift coefficient, or line-mixing parameter) for the collision between an active molecule A and air using the measured A-N_2 and A-O_2 parameters assuming binary collisions and a standard atmospheric composition of air (Tejwani & Varnassi, 1971):

$$G(A - Air) = 0.79G(A - N_2) + 0.21G(A - O_2) \tag{25}$$

3.8 Line-mixing and shift correlation

It should be noted that for the NH_3 molecule, within the measurement errors, almost all line-mixing and -shifts vary linearly with the considered pressures. However for some lines with small rotational energy gaps, the observed shift- and mixing-coefficients exhibit quadratic dependencies on pressure. This situation is more remarkable for strongly overlapped inversion doublets of the ν_4 band which have small inversion splitting $\Delta\sigma_0$ compared to the rotational energy separation. This is illustrated by Fig. 14 for $^{P}{}_{as}P(8,8)$ doublet with a splitting $\Delta\sigma_0$=0.210 cm^{-1}.

This non linear dependence of line-mixing or line shift on pressure can be expressed as (Smith, 1981):

$$\sigma_{s/a} = \sigma_{0s/a} + P\delta_{0s/a} \pm \frac{S_s}{S_a}\frac{\Delta\sigma_0}{4}P^2Y_{s/a}^2, \tag{26}$$

where $S_{s/a}$, $\sigma_{0s/a}$, $\delta_{0s/a}$ and $Y_{s/a}$ are, respectively, the intensity, the unperturbed position, the shift coefficient and line-mixing parameter of the (s) or (a) components of the doublets. The sign (±) is considered for the (s) or (a) transitions of NH_3. This equation illustrates a correlation between line-mixing and shift phenomena. This quadratic evolution of frequency shift with pressure has been also observed previously by Thibault et al. (Thibault et al., 1992) for the 0-1 and 0-2 bands of CO perturbed by He. Also, nonlinear NO-He and NO-Ar shifts have been observed by Vyrodov et al. using laser-induced fluorescence (Vyrodov et al., 1995).

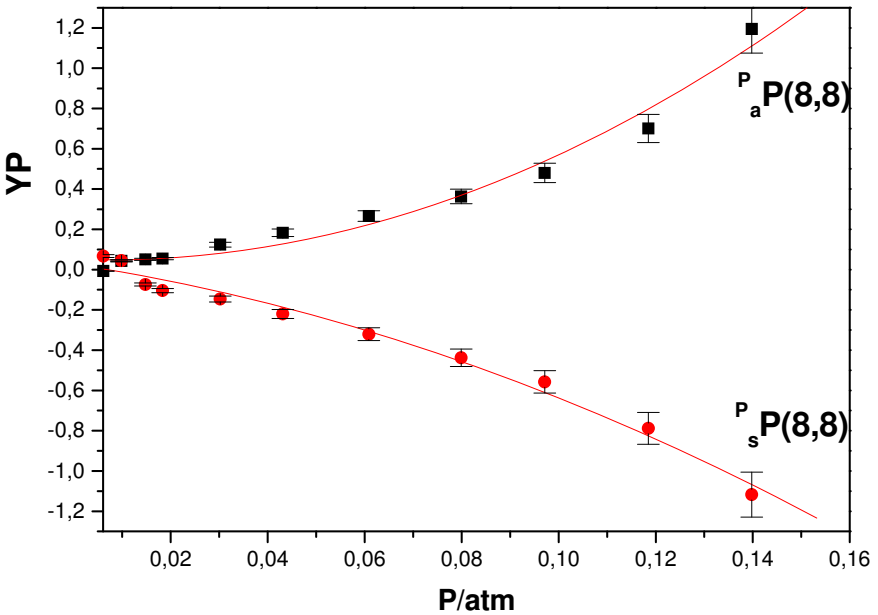

Fig. 14. Variation of PY as function of pressure P for the two components of $^{P}{}_{as}P(8,8)$ doublet of the ν_4 band of NH_3 self-perturbed

3.9 Line parameter accuracies

Considering the unknown systematic uncertainties in sample pressure and temperature, and the absorption path length, the errors are often estimated as one or two standard deviations (1 or 2σ) derived from the linear fits, and vary widely depending on the quality of spectral lines, which is related to the overlapping of neighboring lines and the base line location. The experimental errors reported in Table 3 are estimated as one standard deviation as derived from the linear fit of line mixing and line shifts parameters.

This table also reveals that the line-mixing parameters are more accurate than the shifts. The mean value of accuracy is about 15% for line-mixing parameters and 25% for the shift coefficients that can attain more than 50% or are of the same order of magnitude as the parameter themselves. This makes them negligible and difficult to measure reliably.

Today the achievable accuracies with FTIR are about 3% for line intensities, 5% for pressure broadening coefficients, and 15-20% for pressure-induced line shifts and line-mixing parameters.

It should be noted that, in some instances, the broadening coefficient accuracies of some lines tends to have greater values, which can attain 10-15%. These errors can be explained by the relatively low intensities and the overlaps with neighboring lines.

For the temperature dependence of the broadening coefficients, since the values of temperature coefficient n are determined from a power-law relation, the estimated errors in the derived values of n are larger than the corresponding errors in the measured broadening coefficients. Assuming an error of 5% for broadening measurements, the uncertainty of n values could be about 15%.

4. Conclusion

The purpose of this paper was to highlight and demonstrate the ability of the Fourier Transform Infrared Spectrometer to measure spectroscopic parameters such as line intensities, line broadenings, line shifts and line-mixing parameters for a select number of small molecules.

Compared to the dispersive spectrometers, this technique has the advantage to measure with high precision complete sets of line parameters over large spectral regions.

Fourier transform spectroscopy was used here to study infrared spectra of three molecules: one linear, OCS, and two symmetric tops: NH_3 and CH_3Br which are of considerable interest for quantitative and qualitative studies of planetary and Earth's atmospheres.

These spectra were fitted using a multi-spectrum fitting technique and the first order model absorption coefficient taking into account line-mixing effects. In the considered pressure range, this model is adequate to extract with high enough accuracy line parameters for the studied molecules. For CH_3Br a Voigt profile is used to extract the line parameters, indeed in this case no significant deviations are observed when the measured and calculated spectra are compared.

The estimated errors vary widely depending on the quality of spectral lines with, in general, improving accuracies in the order: line intensities, line broadenings, line-mixing and line

shifts. Among these spectroscopic parameters, the line shifts are the smallest, so are the most difficult to measure with a high accuracy.

More measurements were performed in the ν_2, $2\nu_2$ and ν_4 bands of NH_3 at room temperature and at low temperatures, as well as in the ν_2 and ν_6 bands of CH_3Br and in the $4\nu_2$ band of OCS. However, in the ^PP branch of the ν_4 band of NH_3, the shifts are correlated to the line-mixing parameters and exhibited significant non-linearity. The broadening coefficients do not show any pronounced vibrational effect. For NH_3, the self-shift coefficients are rather large and more bipolar than foreign gas shifts with no significant branch or rotational dependencies.

5. Acknowledgments

The authors are grateful to the "Ministry of Education and Scientific Research in Tunisia" who has supported this work.

6. References

Abrams, M.C., Toons, G.C. & Schindler, R.A., 1994. A practical example of the correction of Fourier transform spectra for detector nonlinearity. *Appl. Opt.,* 33, 6307-6314.

Aliev, M.R., Papousek, D. & Urban, S., 1987. Third-order theory of the line intensities in the allowed and forbidden vibrational-rotational bands of C_{3v} molecules. *J. Mol. Spectrosc.,* 124, 285-305.

Aroui, H. Broquier, M. Picard-Bersellini, A. Bouanich, J.P. Chevalier, M. & Gherissi, S., 1998. Absorption intensities, pressure-broadening and line-mixing parameters of some lines of NH_3 in the ν_4 Band. *J. Quant. Spectrosc. Radiat. Transfer.*, 60, 1011-1023.

Aroui, H., Laribi, H., Orphal, J. & Chelin, P., 2009. Self-broadening, self-shift and self-mixing in the ν_2, $2\nu_2$ and ν_4 bands of NH_3. *J. Quant. Spectrosc. Radiat. Transfer.*, 110, 2037-2059.

Aroui, H., Nouri, S. & Bouanich, J.P., 2003. NH_3 self-broadening coefficients in the ν_2 and ν_4 bands and line intensities in the ν_2 band. *J. Mol. Spectrosc.,* 220, 248-58.

Auwera, J.V., 2004. Agrégation de l'Enseignement Supérieur (HDR thesis), Quantitative high resolution Fourier transform infrared spectroscopy. May, Université libre de Bruxelle.

Babay, A., 1997. Thèse de doctorat. Université des Sciences et Technologies de Lille.

Baldacchini, G., Marchetti, S., Montelatici, V., Buffa, G. & Tarrini, O., 1982. Experimental and theoretical investigations of self-broadening and self-shifting of ammonia transitions in the ν_2 band. *J. Chem. Phys.,* 76, 5271-77.

Bell, R.J., 1972. Introductory Fourier Transform Spectroscopy. *Academic press Inc. New York and London.*

Belov, S.P., Krupnov, A.F., Markov, V.N., Mel'nikov, A.A., Skvortsov, V.A. & Tret'yakov, M.Y., 1982. The study of microwave pressure lineshifts. *J. Mol. Spectrosc.,* 94, 264-82.

Bezard, B., DeBergh, C., Crisp, D. & Maillard, J.P., 1990. The deep atmosphere of Venus revealed by high-resolution nightside spectra. *Nature.,* 345, 508-11.

Bouanich, J.P., Walrand, J., Alberty, S. & Blanquet, G., 1987. Diode-laser measurements of oxygen-broadened line widths in the ν_1 band of OCS. *J Mol Spectrosc.,* 123, 37-47.

Brassewell, R., 1965. The Fourier Transform and its applications. *McGraw-Hill Book Company, New York.*

Brassington, D.J., 1988. I*n Proceedings of International Symposium on Monitoring of gaseous Pollutant by Diode Laser*, Freiburg, Germany, 17 October.

Broquier, M. & Picard-Bersellini, A., 1984. Overlapping effects and collisional narrowing in rotational doublets of OCS in the infrared. *Chem. Phys. Lett.,* 111, 602-06.

Brown, L.R. & Peterson, D.B., 1994. An empirical expression for linewidths of ammonia from far-infrared measurements. *J. Mol. Spectrosc.,* 168, 593–606.

Camy-Peyret, C., Payan, S., Jeseck, P. & Té, Y., 2001. Spectroscopie ultra-sensible des gaz; détection de polluants. C. R. Acad. Sci. Paris., t. 2, Série IV, 905-922.

Cooley, J.W. & Tukey, J.W., 1965. An algorithm for the machine calculation of complex Fourier series, Maths. Comput. 19, 297-301.

Cottaz, C., Tarrago, G., Kleiner, I. & Brown, L.R., 2001. Assignments and intensities of $^{14}NH_3$ hot bands in the 5- to 8-μm ($3\nu_2$-ν_2, ν_2+ν_4-ν_2) and 4μm ($4\nu_2$-ν_2, ν_1-ν_2, ν_3-ν_2 and $4\nu_4$-ν_2) regions. *J. Mol. Spectrosc.,* 209, 30–49.

Davis, S.P., Abrams, M.C. & Brault, J.W., 2001. Fourier Transform Spectroscopy. *Academic press Inc.*

Dello Russo, N., DiSanti, M.A., Mumma, M.J., Magee-Sauer, K. & Rettig, T.W., 1998. Carbonyl sulfide in comets C/1996 B2 (Hyakutake) and C/1995 O1 (Hale-Bopp): evidence for an extended source in Hale-Bopp. *Icarus*., 135, 377-88.

Devi, V.M., Benner, D.C., Brown, L.R., Smith, M.A.H., Rinsland, C.P., Sams, R.L. & Sharpe, S.W., 2002. Multi-spectrum analysis of self- and N_2-broadening, shifting and line-mixing. coefficients in the ν_6 band of $^{12}CH_3D$. *J. Quant. Spectrosc. Radiat. Transfer*., 72, 139-91.

Dhib, M., Aroui, H. & Orphal, J., 2007. Experimental and theoretical study of line shift and mixing in the ν_4 band of NH_3 perturbed by N_2. *J. Quant. Spectrosc. Radiat. Transfer*., 107, 372-84.

Dhib, M., Echargui, M.A., Aroui, H. & Orphal, J., 2006. Shifting and line-mixing parameters in the ν_4 band of NH_3 perturbed by CO_2 and He: experimental results and theoretical calculations. *J. Mol. Spectrosc.,* 238, 168-77.

Domenech, J.L., Bermejo, D., & Bouanich, J.P., 2000. Pressure lineshift and broadening coefficients in the $2\nu_3$ band of $^{16}O^{12}C^{32}S$. *J Mol Spectrosc*., 200, 266-76.

Evans, N.J., Lacy, J.H. & Carr, J.S., 1991. Infrared molecular-spectroscopy toward the Orion IRC2 and IRC7 sources: a new probe of physical conditions and abundances in molecular clouds. *Astrophys J.,* 383, 674-92.

Fabian, M. & Yamada, K.M.T., 1999. Absolute Intensity of the NH_3 ν_2 Band. *J. Mol. Spectrosc.,* 198, 102-109.

Galalou, S., Ben Mabrouk, K., Aroui, H., Kwabia Tchana, F., Willaert, F. & Flaud, J-M., 2011. N_2 and O_2 Pressure Broadening and Pressure Shift in the $4\nu_2$ Band of $^{16}O^{12}C^{32}S$. *J. Quant. Spectrosc. Radiat. Transfer*., 112 , 2750-2761.

Gentry, G. & Larrabee Strow, L., 1987. Line-mixing in a N_2-broadened CO_2 Q branch observed with a tunable diode laser. *J. Chem. Phys.,* 86, 5722–30.

Giraud, M., Robert, D. & Galatry, L., 1971. Sur la détermination du moment quadrupolaire de molecules linéaires à partir de l'élargissement des raies spectrales. *C.R. Acad. Sci. Paris.,* 272, 1252–55.

Gomez, L., Jacquemart, D., Bouanich, J.P., Boussetta, Z. & Aroui, H., 2010. Theoretical calculations of self-broadening coefficients in the ν_6 band of CH_3Br. *J. Quant. Spectrosc. Radiat. Transfer*., 111, 1252-1261.

Griffiths, P.R. & de Haseth, J.A., 1986. Fourier Transform Infrared Spectroscopy. *Wiley, New York*.

Guelachvili, C., 1986. Distortion-free interferograms in Fourier transform spectroscopy with nonlinear detectors. *Appl. Opt*. 25, 4644-48.

Hadded, S., Aroui, H., Orphal, J., Bouanich, J.P. & Hartmann, J.M., 2001. Line broadening and mixing in NH_3 inversion doublets perturbed by NH_3, He, Ar, and H_2. *J Mol Spectrosc*., 210, 275-83.

Hartmann, J.M., Bouanich, J.P., Blanquet, G., Walrand, J. & Lacome, N., 1995. Simple modeling of Q branch absorption-II: application to molecules of atmospheric interest. *J. Quant. Spectrosc. Radiat. Transfer*., 54, 723-35.

Ho, P.T.P. & Townes, C.H., 1983. Interstellar Ammonia. *Ann. Rev. Astr. Astrophys.,* 21, 239-270.

Jacquemart, D., Kwabia Tchana, F., Lacome, N. & Kleiner, I., 2007. A complete set of line parameters for CH_3Br in the 10 μm spectral region. *J. Quant. Spectrosc. Radiat. Transfer.,* 105, 264–302.

Jacquinet-Husson, N., Scott, N.A., Chédin, A., Garceran, K., Armante, R., Chursin, A.A. et al., 2005. The 2003 edition of the GEISA/IASI spectroscopic database. *J. Quant. Spectrosc. Radiat. Transfer*. 95, 429-67.

Kleiner, I., Brown, L.R., Tarrago, G., Kou, Q.L., Picqué, N., Guelachvili, G. Dana, V. & Mandin, J.Y., 1999. Positions and intensities in the $2\nu_4/\nu_1/\nu_3$ vibrational system of $^{14}NH_3$ near 3 μm. *J. Mol. Spectrosc.,* 193, 46-71.

Kleiner, I., Tarrago, G., Cottaz, C., Sagui, L., Brown, L.R., Poynter, R.L., Pickett, H.M., Chen, P., Pearson, J.C., Sams, R.L., Blake, G.A., Matsuura, S., Nemtchinov, V., Varanasi, P., Fusina, L. & Lonardo, G. Di., 2003. NH_3 and PH_3 line parameters: the 2000 HITRAN update and new results. *J. Quant. Spectrosc. Radiat. Transfer*., 82, 293-312.

Koshelev, M.A. & Tretyakov, M.Y., 2009. Collisional broadening and shifting of OCS rotational spectrum lines. *J. Quant. Spectrosc. Radiat. Transfer*., 110, 118-28.

Koshelev, M.A., Tretyakov, M.Y., Lees, R.M. & Xu, L.H., 2006. Tunable diode laser measurements of N_2- and O_2-pressure broadening and pressure-induced shifts for $^{16}O^{12}C^{32}S$ transitions in the ν_3 band. *J Mol Struc*., 780-781, 7-16.

Kunde, V., Hanel, R., Maguire, W., Gautier, D., Baluteau, J.P., Marten, A., Chedin, A., Husson, N. & Scott, N., 1982. The tropospheric gas composition of Jupiter's north equatorial belt /NH_3, PH_3, CH_3D, GeH_4, H_2O/ and the Jovian D/H isotopic ratio. Astrophysical J., 263, 443-467.

Kurylo, M.J. & Rodriguez, J.M., 1999. Chapter 2, Short-lived Ozone-Related Compounds. In: Scientific Assessment of Ozone Depletion: 1998. Global Ozone Research and Monitoring. *Project - Report 44, WMO, Geneva, Switzerland*, 21-56.

Lévy, A., Lacome, N. & Chackerian, C.Jr., 1992. Spectroscopy of the Earth's Atmosphere and Interstellar Medium. *Academic Press, New York*, 261-337.

Markov, V.N., Pine, A.S., Buffa, G. & Tarrini, O., 1993. Self broadening in the ν_1 band of NH_3. *J. Quant. Spectrosc. Radiat. Transfer*., 50, 167-78.

Martin, S., Martin-Pintado, J., Mauersberger, R., Henkel C. & Garcia-Burillo, S., 2005. Sulfur chemistry and isotopic ratios in the Starburst Galaxy NGC 253. *Astrophys J.*, 620, 210-216.

Mauersberger, R., Henkel, C. & Chin, Y.N., 1995. Dense gas in nearby galaxies viii. The detection of OCS. *Astron Astrophys.,* 294, 23-32.

McElroy, M.B., Salawitch, R.J., Wosfy, S.C., & Logan, J.A., 1986. Antarctic ozone: Reductions due to synergistic interactions of chlorine and bromine. *Lett. Nat.*, 321, 759-762.

Mertz, L., 1965. Transformations in optics. New York: Wiley.

Mouchet, A., Blanquet, G., Herbin, P., Walrand, J., Courtoy, C.P. & Bouanich, J.P., 1985. Diode laser measurements of N_2-broadened line widths in the ν_1 band of OCS. *Can J Phys.*, 63, 527-31.

Nemtchinov, V., Sung, K. & Varanasi, P., 2004. Measurements of line intensities and half-widths in the 10 μm bands of NH_3. *J. Quant. Spectrosc. Radiat. Transfer.*, 83, 243-65.

Nouri, S., Aroui, H., Bouanich, J.P., Orphal, J. & Hartmann, J.M., 2004. Temperature dependence of pressure broadening of NH_3 perturbed by H_2 and N_2. *J. Mol. Spectrosc.*, 227, 60-66.

Ozanne, L., Bouanich, J.P., Rodrigues, R., Hartmann J.M., Blanquet G. & Walrand J., 1999. Diode laser measurements of He and N_2 broadening coefficients and line-mixing effects in the Q branch of the ν_1-ν_2 band of CO_2. *J. Quant. Spectrosc. Radiat. Transfer.*, 61, 153–84.

Perrin, A., Puzzarini, C., Colmont, J-M., Verdes, C., Wlodarczak, G., Cazzoli, G. & al., 2005. Molecular line parameters for the ''MASTER'' (millimeter wave acquisitions for stratosphere/troposphere exchange research) database. *J Atmos Chem.* 51, 161-205.

Pickett, H.M., Poynter, R.L., Cohen, E.A., Delitsky, M.L., Pearson, J.C. & Muller, H.S.P., 1998. Submillimeter, millimeter, and microwave spectral line catalog. *J. Quant. Spectrosc. Radiat. Transfer.* 60, 883-90.

Pieroni, D., Nguyen, V.T., Brodbeck, C., Claveau, C., Valentin, A., Hartmann, J.M., Gabard, T., Champion, J.P., Bermejo, D. & Domenech, J.L., 1999. Experimental and theoretical study of line-mixing methane spectra. I. The N_2- broadened ν_3 band at room temperature. *J. Chem. Phys.*, 110, 7717–32.

Pine, A.S. & Markov, V.N., 2004. Self- and foreign-gas-broadened lineshapes in the ν_1 band of NH_3. *J. Mol. Spectrosc.*, 228, 121–42.

Pine, A.S., 1997. N_2 and Ar broadening and line-mixing in the P and R branches of the ν_3 band of CH_4. *J. Quant. Spectrosc. Radiat. Transfer*., 57, 157-176.

Pourcin, J., Jacquemoz, A., Fournel, A. & Sielmann, H., 1981. Pressure broadening of HCl pure rotational lines with a far-infrared optically pumped laser. *J. Mol. Spectrosc.*, 90, 43–50.

Raynaud, F., Lemoine, B. & Rohart, F., 1994. High precision pressure-induced lineshifts measured with a frequency-stabilized diode laser: application to ν_2 and ($2\nu_2$-ν_2) bands of NH_3. *J. Mol. Spectrosc.*, 168, 584-92.

Rinsland, C.P., Devi, V.M., Chris Benner, D., Blake, T.A., Sams, R.L., Brown, L.R., Kleiner, I., Dehayem-Kamadjeu, A., Müller, H.S.P., Gamache, R.R., Niles, D.L. & Masiello, T., 2008. Multi-spectrum analysis of the ν_4 band of CH_3CN: Positions, intensities, self and N_2-broadening, and pressure induced shifts. *J. Quant. Spectrosc. Radiat. Transfer.*, 109, 974-94.

Rosenkranz, P.W., 1975. Shape of the 5mm oxygen band in the atmosphere. *IEEE Trans. Antennas Propag.*, 23, 498-506.

Rothman, L.S., Gordon, I.E., Barbe, A., Benner, D.C., Bernath, P.F., Birk, M., Boudon, V., Brown, L.R., Campargue, A., Champion, J.P., Chance, K., Coudert, L.H., Dana, V., Devi, V.M., Fally, S., Flaud, J-M., Gamache, R. R., Goldman, A., Jacquemart, D., Kleiner, I. et al., 2009. The HITRAN 2008 molecular spectroscopic database. *J. Quant. Spectrosc. Radiat. Transfer*. 110, 533-72.

Smith, E.W., 1981. Absorption and dispersion in the O_2 microwave spectrum at atmospheric pressures. *J. Chem. Phys.*, 74, 6658–6673.

Tejwani, G.D.T. & Varnassi, P., 1971. Theoretical line widths in N_2O-N_2O and N_2O-air collisions. *J. Quant. Spectrosc. Radiat. Transfer.*, 11, 1659-64.

Thibault, F., Boissoles, B., Grigoriev, I.M., Filippov, N.N. & Tonkov, M.V., 1999. Line-mixing effects in the ν_3 band of CH_3F in helium: experimental band shapes and ECS analysis. *Eur. Phys. J. D.*, 6, 343-53.

Thibault, F., Boissoles, J., Le Doucen, R., Farrenq, R., Morillon-Chapey, M. & Boulet, C., 1992. Line by line measurements of interference parameters for the 0-1 and 0-2 bands of CO in He, and comparison with coupled-states calculations. *J. Chem. Phys.*, 97, 4623-32.

Thomas, V.M., Bedford, J.A. & Cicerone, R.J., 1997. Bromine emissions from leaded gasoline. *Geophys. Res. Lett.*, 24, 1371–1374.

Tran, H. Jacquemart, D., Mandin, J.Y. & Lacome, N., 2008. Line mixing in the ν_6 Q branches of self-and nitrogen-broadened methyl bromide. *J. Quant. Spectrosc. Radiat. Transfer.*, 109, 119-31.

U.S. Environmental Protection Agency, 2011. Gaseous Pollutants - Fourier Transform Infrared Spectroscopy (FTIR)

Vyrodov, A.O., Heinze, J. & Meier U.E., 1995. Collisional broadening of spectral lines in the A-X system of NO by N_2, Ar and He at elevated pressure measured by laser-induced fluorescence. *J. Quant. Spectrosc. Radiat. Transfer.*, 53, 277-87.

Wartewig, S., 2003. IR and Raman spectroscopy: fundamental processing. *Weinheim: Wiley-VCH*.

Watson, J.K.G., 1992. Quadratic Herman-Wallis factors for symmetric- and asymmetric-top molecules. *J. Mol. Spectrosc.*, 153, 211-24.

Watts, S.F., 2000. The mass budgets of carbonyl sulfide, dimethyl sulfide, carbon disulfide and hydrogen sulfide. *Atmos Environ.*, 34, 761-79.

Woodney, L.M., McMullin, J. & Ahearn, M.F., 1997. Detection of OCS in comet Hyakutake, (C/1996 B2). *Planet Space Sci.*, 45, 717-9.

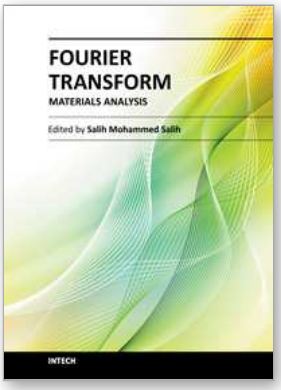

Fourier Transform - Materials Analysis

Edited by Dr Salih Salih

ISBN 978-953-51-0594-7
Hard cover, 260 pages
Publisher InTech
Published online 23, May, 2012
Published in print edition May, 2012

The field of material analysis has seen explosive growth during the past decades. Almost all the textbooks on materials analysis have a section devoted to the Fourier transform theory. For this reason, the book focuses on the material analysis based on Fourier transform theory. The book chapters are related to FTIR and the other methods used for analyzing different types of materials. It is hoped that this book will provide the background, reference and incentive to encourage further research and results in this area as well as provide tools for practical applications. It provides an applications-oriented approach to materials analysis written primarily for physicist, Chemists, Agriculturalists, Electrical Engineers, Mechanical Engineers, Signal Processing Engineers, and the Academic Researchers and for the Graduate Students who will also find it useful as a reference for their research activities.

How to reference

In order to correctly reference this scholarly work, feel free to copy and paste the following:

Hassen Aroui, Johannes Orphal and Fridolin Kwabia Tchana (2012). Fourier Transform Infrared Spectroscopy for the Measurement of Spectral Line Profiles, Fourier Transform - Materials Analysis, Dr Salih Salih (Ed.), ISBN: 978-953-51-0594-7, InTech, Available from: http://www.intechopen.com/books/fourier-transform-materials-analysis/fourier-transform-infrared-spectroscopy-for-the-measurement-of-spectral-line-profiles

INTECH
open science | open minds

InTech Europe
University Campus STeP Ri
Slavka Krautzeka 83/A
51000 Rijeka, Croatia
Phone: +385 (51) 770 447
Fax: +385 (51) 686 166
www.intechopen.com

InTech China
Unit 405, Office Block, Hotel Equatorial Shanghai
No.65, Yan An Road (West), Shanghai, 200040, China
中国上海市延安西路65号上海国际贵都大饭店办公楼405单元
Phone: +86-21-62489820
Fax: +86-21-62489821